Anti-Biofouling Properties of Comblike Block Copolymers with Amphiphilic Side Chains

Sitaraman Krishnan,[†] Ramakrishnan Ayothi,[†] Alexander Hexemer,[‡] John A. Finlay,[||] Karen E. Sohn,[‡] Ruth Perry,[||] Christopher K. Ober,*[,†] Edward J. Kramer,[‡,§] Maureen E. Callow,[||] James A. Callow,[||] and Daniel A. Fischer[⊥]

Department of Materials Science and Engineering, Cornell University, Ithaca, New York 14853, Department of Materials and Department of Chemical Engineering, University of California at Santa Barbara, Santa Barbara, California 93106, School of Biosciences, The University of Birmingham, Edgbaston, Birmingham B15 5TT, U.K., and National Institute of Standards and Technology, Gaithersburg, Maryland 20899

Received November 5, 2005. In Final Form: January 29, 2006

Surfaces of novel block copolymers with amphiphilic side chains were studied for their ability to influence the adhesion of marine organisms. The surface-active polymer, obtained by grafting fluorinated molecules with hydrophobic and hydrophilic blocks to a block copolymer precursor, showed interesting bioadhesion properties. Two different algal species, one of which adhered strongly to hydrophobic surfaces, and the other, to hydrophilic surfaces, showed notably weak adhesion to the amphiphilic surfaces. Both organisms are known to secrete adhesive macromolecules, with apparently different wetting characteristics, to attach to underwater surfaces. The ability of the amphiphilic surface to undergo an environment-dependent transformation in surface chemistry when in contact with the extracellular polymeric substances is a possible reason for its antifouling nature. Near-edge X-ray absorption fine structure spectroscopy (NEXAFS) was used, in a new approach based on angle-resolved X-ray photoelectron spectroscopy (XPS), to determine the variation in chemical composition within the top few nanometers of the surface and also to study the surface segregation of the amphiphilic block. A mathematical model to extract depth-profile information from the normalized NEXAFS partial electron yield is developed.

1. Introduction

Marine surfaces have a tendency to rapidly accumulate colonizing organisms that may range from microscopic bacteria, cyanobacteria, spores of algae, and unicellular eukaryotes such as diatoms to larger larvae of invertebrates. Colonization starts within minutes to hours of immersion of the surface in water, which is followed by the formation of a biofilm consisting of firmly attached cells.[1] Attached algal spores or invertebrate larvae rapidly grow into macroscopic adults. The accumulation of biomass on a ship hull due to the above process is undesirable from the point of view of higher hydrodynamic drag resulting in lower operational speeds or increased fuel consumption.[2] The toxic paints used to prevent biofouling raised concerns that they were adversely affecting the marine ecosystem by leaching certain metals that bioaccumulate.[3] A more environmentally friendly approach is to use nontoxic coatings that can resist colonization by fouling organisms or minimize the strength of adhesion of those organisms that do attach and grow on the surface. Both the settlement and adhesion of marine cells are affected by chemical,[4−6] topographic,[7,8] and biological[9] cues and can vary from one species to another. Previous studies[4,5,7−10] have focused on understanding the role of these cues in the attachment of zoospores (the microscopic colonizing stage) of the green macroalga *Ulva linza* (syn. *Enteromorpha linza*[11]) to surfaces. The quadriflagellate, motile, pear-shaped, asexual zoospores of *Ulva* settle on a surface by a process of selection and germinate after attachment to form young plants ("sporelings"). The selection process involves several steps of reversible attachment to and sensing of the surface until an optimal surface is found for permanent attachment.[12] Attachment is achieved through secretion of a glycoprotein adhesive that is present in a highly condensed form within vesicles inside the spore,[13] followed by cross linking with a corresponding increase in the adhesion strength. It is now known that although settlement of the zoospores is strongly promoted by a hydrophobic poly(dimethyl siloxane) (PDMS) surface the attachment strength of both the spores and sporelings is significantly weaker than on a hydrophilic glass substrate.[5,14] This is a favorable aspect from the standpoint of currently used

* To whom correspondence should be addressed. E-mail: cober@ccmr.cornell.edu. Tel: 607-255-8417. Fax: 607-255-2365.

[†] Cornell University.

[‡] Department of Materials, University of California at Santa Barbara.

[§] Department of Chemical Engineering, University of California at Santa Barbara.

[||] The University of Birmingham.

[⊥] National Institute of Standards and Technology.

(1) Callow, J. A.; Callow, M. E. Biofilms. In *Antifouling Compounds. Progress in Molecular and Subcellular Biology: Marine Molecular Biotechnology;* Fusetani, N., Clare, A. S., Eds.; Springer: New York, in press.

(2) Townsin, R. L. *Biofouling* **2003**, *19*(Supplement), 9−15.

(3) Clark, E. A.; Sterritt, R. M.; Lester, J. N. *Environ. Sci. Technol.* **1988**, *22*, 600−604.

(4) Callow, J. A.; Callow, M. E.; Ista, L. K.; Lopez, G. Chaudhury, M. K. *J. R. Soc. Interface* **2005**, *2*, 319−325.

(5) Finlay, J. A.; Callow, M. E.; Ista, L. K.; Lopez, G. P.; Callow, J. A. *Integr. Comput. Biol.* **2002**, *42*, 1116−1122.

(6) Wigglesworth-Cooksey, B.; van der Mei, H.; Busscher, H. J.; Cooksey, K. E. *Colloids Surf., B* **1999**, *15*, 71−80.

(7) Callow, M. E.; Jennings, A. R.; Brennan, A. B.; Seegert, C. E.; Gibson, A.; Wilson, L.; Feinberg, A.; Baney, R.; Callow, J. A. *Biofouling* **2002**, *18*, 237−245.

(8) Hoipkemeier-Wilson, L.; Schumacher, J. F.; Carman, M. L.; Gibson, A. L.; Feinberg, A. W.; Callow, M. E.; Finlay, J. A.; Callow, J. A.; Brennan, A. B. *Biofouling* **2004**, *20*, 53−63.

(9) Tait, K.; Joint, I.; Daykin, M.; Milton, D. L.; Williams, P.; Cámara, M. *Environ. Microbiol.* **2005**, *7*, 229−240.

(10) Youngblood, J. P.; Andruzzi, L.; Ober, C. K.; Hexemer, A.; Kramer, E. J.; Callow, J. A.; Finlay, J. L.; Callow, M. E. *Biofouling* **2003**, *19*, 91−98.

(11) The genus *Enteromorpha* has recently been incorporated into the genus *Ulva*. See Hayden, H. S.; Blomster, J.; Maggs, C. A.; Silva, P. C.; Stanhope, M. J.; Waal, J. R. *Eur. J. Phycol.* **2003**, *38*, 277−294.

(12) Callow, M. E.; Callow, J. A. *Biofouling* **2000**, *15*, 49−56.

(13) Stanley, M. S.; Callow, M. E.; Callow, J. A. *Planta* **1999**, *210*, 61−71.

10.1021/la052978l CCC: $33.50
Published on Web 04/21/2006

PDMS antifouling coatings. PDMS elastomers are widely used in commercial foul-release coatings because of their combination of properties such as low surface energy, low microroughness, and low modulus. *Ulva* sporelings are released readily from PDMS.[15,16] In contrast, diatoms (unicellular algae) show strong adhesion to PDMS,[17] and it is well known that marine biofilms dominated by diatoms are not releasd easily from PDMS-based fouling-release coatings.[18] A key challenge in marine antifouling research, therefore, is to find a surface that is resistant to fouling by both organisms.

The difference in the adhesion strength between the green macroalga *Ulva* and diatoms could possibly be due to differences in surface interactions of the adhesive extracellular polymeric substances (EPS) secreted by the two organisms. The proteins, glycoproteins, and heteropolysaccharides in EPS are likely to be amphiphilic, with both hydrophobic and hydrophilic functionalities. When such a macromolecule comes into contact with a surface, it can undergo conformational change, thereby exposing different functionalities to optimize adsorption at the substrate.[4] Gudipati et al.[19] hypothesized that optimal nanoscale topographical and compositional complexities of a surface would make it energetically unfavorable for protein or glycoprotein adsorption, thereby weakening the adhesion strength of the entire organism with the surface. They found that amphiphilic networks containing hyperbranched fluoropolymers cross linked with poly(ethylene glycol) (PEG) produced this kind of surface. Phase segregation of the fluoropolymer and PEG domains took place and resulted in a higher release of *Ulva* sporelings compared to PDMS. Similar amphiphilic networks prepared from hydrophobic polyisobutylene and hydrophilic poly(2-hydroxyethyl methacrylate) or poly(*N*,*N*-dimethylacrylamide) were found to exhibit reduced protein adsorption and cell adhesion.[20,21] Kim et al.[22] have used the microphase-separated surface structures of an amphiphilic interpenetrating polymer network (IPN) of polystyrene and polyurethane to prepare biomaterials resistant to platelet adhesion. By changing the amphiphilic balance and controlling microphase separation, they obtained a surface on which collagen adsorbed without undergoing aggregation or conformational changes. The collagen that possessed cell-binding moieties resulted in good endothelial cell adhesion and growth. The nonthrombogenic properties of PEGylated surfaces are well known. For example, Freij-Larsson et al.[23] prepared amphiphilic graft copolymers with hydrophobic styrene blocks and hydrophilic blocks with PEG side chains and observed a reduction in the adsorption of blood proteins.

Our approach, in contrast, is to prepare novel block copolymers with amphiphilic side chains, schematically shown in Figure 1. The use of PEG and fluoroalkyl units for the amphiphilic side chains was motivated by the fact that in initial experiments diatoms

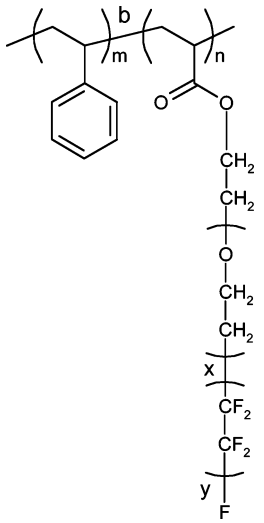

Figure 1. Comblike block copolymer with amphiphilic side chains.

showed a higher release from surfaces of polymers with PEG side chains compared to that with semifluorinated side chains,[24] whereas *Ulva* sporelings showed the opposite behavior.[10,24] It was hypothesized that an amphiphilic surface might result in low adhesion strength of both *Ulva* and *Navicula*. Using a bilayer coating strategy, it is possible to control the modulus and surface chemistry of the coatings independently and also to have a sufficiently thick polymer film without using excessive amounts of the surface-active block copolymer (SABC).[25] The bottom layer of this coating is a polystyrene-*block*-poly(ethylene-*ran*-butylene)-*block*-polystyrene (SEBS, Kraton G1652), and the top layer is the block copolymer shown in Figure 1. The role of the polystyrene block in the SABC is to increase the compatibility of the SEBS and SABC layers by entrapment in the cylindrical polystyrene domains at the SEBS surface.

Amphiphilic block copolymers of ethylene oxide and fluorinated methacrylate have been recently studied by Hussain et al.[26] Also, Vaidya and Chaudhury[27] have investigated the surface properties of amphiphilic polyurethanes prepared by reacting fluorinated diols with isocyanate-terminated poly(ethylene oxide)-*block*-poly(dimethyl siloxane)-*block*-poly(ethylene oxide). However, the polymer architecture shown in Figure 1 is different from those of the polymers in Hussain et al.,[26] Vaidya and Chaudhury,[27] and Gudipati et al.[19] in that it would allow environment-dependent surface reconstruction by simple flipping of the side chains, as depicted in Figure 2. Other architectures would require mesoscale rearrangement of the hydrophobic and hydrophilic domains to effect a similar polarity change. Moreover, one would expect that if the surface is covered with a thin layer of the ethoxylated fluoroalkyl side chains, as shown in Figure 2, any change in surface polarity would occur uniformly throughout the surface, without the complex topographic changes observed by others.[21,28]

In this report, we begin with a description of the synthesis of the block copolymer and the fabrication of surfaces. This is followed by a discussion of contact angle measurements, near-

(14) Finlay, J. A.; Callow, M. E.; Schultz, M. P.; Swain, G. W.; Callow, J. A. *Biofouling* **2002**, *18*, 251−256.
(15) Schultz, M. P.; Finlay, J. A.; Callow, M. E.; Callow, J. A. *Biofouling* **2003**, *19*(Supplement), 17−26.
(16) Chaudhury, M. K.; Finlay, J. A.; Chung, J. Y.; Callow, M. E.; Callow, J. A. *Biofouling* **2005**, *21*, 41−48.
(17) Holland, R.; Dugdale, T. M.; Wetherbee, R.; Brennan, A. B.; Finlay, J. A.; Callow, J. A.; Callow, M. E. *Biofouling* **2004**, *20*, 323−329.
(18) Terlizzi, A.; Conte, E.; Zupo, V.; Mazzella, L. *Biofouling* **2000**, *15*, 327−342.
(19) Gudipati, C. S.; Finlay, J. A.; Callow, J. A.; Callow, M. E.; Wooley, K. L. *Langmuir* **2005**, *21*, 3044−3053.
(20) Keszler, B.; Kennedy, J. P.; Ziats, N. P.; Brunstedt, M. R.; Yun, J. K.; Anderson, J. M. *Polym. Bull.* **1992**, *29*, 681−688.
(21) Park, D.; Keszler, B.; Galiatsatos, V.; Kennedy, J. P.; Ratner, B. D. *Macromolecules* **1995**, *28*, 2595−2601.
(22) Kim, J. H.; Kim, S. H.; Kim, H. K.; Akaike, T.; Kim, S. C. *J. Biomed. Mater. Res.* **2002**, *62*, 613−621.
(23) Freij-Larsson, C.; Nylander, T.; Jannasch, P.; Wesslén, B. *Biomaterials* **1996**, *17*, 2199−2207.
(24) Krishnan, S.; Wang, N.; Ober, C. K.; Finlay, J. A.; Callow, M. E.; Callow, J. A.; Hexemer, A.; Sohn, K. E.; Kramer, E. J.; Fischer, D. A. *Biomacromolecules*, in press.
(25) Hexemer, A.; Sivaniah, E.; Kramer, E. J.; Xiang, M.; Li, X.; Fischer, D. A.; Ober, C. K. *J. Polym. Sci., Part B: Polym. Phys.* **2004**, *42*, 411−420.
(26) Hussain, H.; Kerth, A.; Blume. A.; Kressler, J. *J. Phys. Chem. B* **2004**, *108*, 9962−9969.
(27) Vaidya, A.; Chaudhury, M. K. *J. Colloid Interface Sci.* **2002**, *249*, 235−245.
(28) Gudipati, C. S.; Greenlief, C. M.; Johnson, J. A.; Pornpimol, P.; Wooley, K. L. *J. Polym. Sci., Part A: Polym. Chem.* **2004**, *42*, 6193−6208.

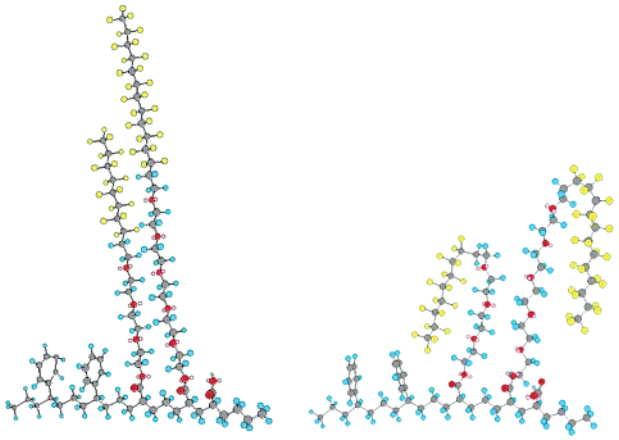

Figure 2. Proposed mechanism for surface reconstruction of the ethoxylated fluoroalkyl side chains upon immersion of the surface in water. The picture on the left indicates the orientation of side chains in air whereas that on the right shows the effect of water immersion.

edge X-ray absorption fine structure (NEXAFS) spectroscopy, X-ray photoelectron spectroscopy (XPS), and scanning force microscopy (SFM) experiments, which were used to understand the chemical composition and morphology of the surfaces. The final section discusses the fouling-release properties of the coatings studied using *Ulva* and *Navicula*.

2. Experimental Section

2.1. Materials and Methods. Styrene (CAS no. 100-42-5, FW 104.15, Aldrich, 99%) was passed through a column of basic alumina to remove the 4-*tert*-butylcatechol inhibitor. *Tert*-butyl acrylate (*t*BA, CAS no. 1663-39-4, FW 128.17, Aldrich, 98%) containing 10−20 ppm of monomethyl ether hydroquinone as the inhibitor was extracted with 5% aqueous NaOH and then washed with distilled water. After drying over calcium chloride, the monomer was distilled under vacuum. Copper(I) bromide (CAS no. 7787-70-4, CuBr, FW 143.45, Aldrich, 99.999%), copper(II) bromide (CAS no. 7789-45-9, $CuBr_2$, FW 223.35, Aldrich, 99.999%), 1,1,4,7,7-pentamethyldiethylenetriamine (PMDETA, CAS no. 3030-47-5, $[(CH_3)_2NCH_2CH_2]_2NCH_3$, FW 173.30, Aldrich, 99%), methyl 2-bromopropionate (MBP, CAS no. 5445-17-0, $CH_3CHBrCOOCH_3$, FW 167.00, Aldrich, 98%), 1,3-dicyclohexylcarbodiimide (DCC, CAS no. 538-75-0, $C_6H_{11}N{=}C{=}NC_6H_{11}$, FW 206.33, Aldrich, 99%), 4-(dimethylamino)pyridine (DMAP, CAS no. 1122-58-3, $(CH_3)_2NC_5H_4N$, FW 122.17, Aldrich, 99%), anhydrous pyridine (99.8%), acetone (99.5%), and anhydrous tetrahydrofuran (THF) were obtained from Sigma-Aldrich and used without further purification. The ethoxylated fluoroalkyl surfactant, Zonyl FSO-100 (registered trademark of E. I. du Pont de Nemours & Co., Inc.; CAS no. 122525-99-9), was also obtained from Sigma-Aldrich. The average molecular weight of Zonyl FSO-100, $F(CF_2CF_2)_y(CH_2CH_2O)_xCH_2CH_2OH$ (x = 0−15 and y = 1−7), reported by the supplier is 725 g/mol. 3-(Glycidoxypropyl)-trimethoxysilane (GPS, CAS no. 2530-83-8) was purchased from Gelest. Polystyrene-*block*-poly(ethylene-*co*-butylene)-*block*-polystyrene (SEBS) triblock thermoplastic elastomer (Kraton G1652M) and SEBS grafted with maleic anhydride (MA-SEBS, Kraton FG1901X) were received from Kraton polymers. Methanol, toluene (technical grades, Fisher), 96% sulfuric acid, 30 wt % hydrogen peroxide in water, 95% ethanol, and all other reagents were used as received.

2.2. Polymer Synthesis and Characterization. The synthetic scheme is illustrated in Scheme 1.

Poly(tert-butyl acrylate) Macroinitiator (I). A mixture of 3 mL of acetone, 80 mmol of *t*BA, and 0.8 mmol of PMDETA, which was deoxygenated by purging with nitrogen, was added to 0.8 mmol of CuBr and 0.04 mmol of $CuBr_2$ in a round-bottomed flask. After complex formation, which was evident from the change in the appearance of the solution from colorless to clear and light green, 1.6 mmol of MBP was added using a syringe, and the monomer was polymerized for 6 h at 60 °C. After cooling the reaction mixture to room temperature, 50 mL of acetone was added, and the polymer solution was treated with neutral alumina to remove the copper salts. Acetone was removed by evaporation, and the polymer was further purified by dissolving in diethyl ether and precipitating in a methanol/water mixture (1:1 v/v) at 0 °C. Drying under vacuum resulted in a polymer with a molecular weight of about 3000 g/mol and a polydispersity index of 1.1.

^{1}H NMR (300 MHz, $CDCl_3$, δ): 1.5 (s, 9H, −C(CH_3)$_3$); 1.85 and 2.35 (br s, −CH_2−, >C*H*−); 3.75 (s, 3H, −OCH_3 from initiator); 4.1 (m, 1H, >C*H*−Br). IR (dry film) $\tilde{\nu}_{max}$ (cm^{-1}): 2977 (C−H stretching, *tert*-butyl); 2929 (C−H stretching, backbone); 1727 (C═O stretching, ester); 1367 (C−H bending, *tert*-butyl).

Poly(tert-butyl acrylate)-block-polystyrene (II). Two grams (0.67 mmol) of the bromo-terminated poly(*t*BA) and 0.95 mmol of CuBr were taken in a round-bottomed flask. Ninety-five millimoles of deoxygenated styrene was added to the reactor and stirred until it dissolved the polymer. PMDETA (0.95 mmol) was injected to form a complex with CuBr. Polymerization at 100 °C for 120 min resulted in a viscous liquid that was dissolved in 150 mL of tetrahydrofuran after cooling to room temperature. The solution was passed through a column of neutral alumina to remove copper salts, concentrated by evaporation of the solvent, and precipitated in excess of methanol. After reprecipitation in methanol, the polymer was dried under vacuum at room temperature. Gel permeation chromatography indicated a polydispersity index of 1.1.

^{1}H NMR (300 MHz, $CDCl_3$, δ): 1.5 (s, 9H, −C(CH_3)$_3$); 1.85 and 2.35 (br s, −CH_2−, >C*H*−); 6.5 and 7.1 (br s, 5H, styrene). IR (dry film) $\tilde{\nu}_{max}$ (cm^{-1}): 3026 (C−H stretching, aromatic); 2976 (C−H stretching, *tert*-butyl); 2926 (C−H stretching, backbone); 1728 (C═O stretching, ester); 1493, 1452 (C−H bending, backbone); 1600 (C═C stretching, aromatic); 1367 (C−H bending, *tert*-butyl); 758 and 700 (C−H bending, aromatic).

Poly(acrylic acid)-block-polystyrene (III). Two milliliters of concentrated hydrochloric acid solution (12 N) was added to a 10% w/v solution of poly(*tert*-butyl acrylate)-*block*-polystyrene in dioxane, and the solution was refluxed for about 6 h. The polymer was recovered by cooling the dioxane solution and precipitating it from water. Complete hydrolysis of *tert*-butyl acrylate was confirmed by the disappearance of IR absorbances at 2976 and 1367 cm^{-1} corresponding to C−H stretching and bending, respectively, of the *tert*-butyl groups.

^{1}H NMR (300 MHz, DMSO-d_6, δ): 2.2 and 1.6 (br s, −CH_2−, >C*H*−); 6.5 and 7.1 (br s, 5H, styrene); 12.0 (br s, COO*H*). IR (dry film) $\tilde{\nu}_{max}$ (cm^{-1}): 3600−2400 (O−H stretching, carboxylic acid); 3026 (C−H stretching, aromatic); 2926 (C−H stretching, backbone); 1716 (C═O stretching, ester); 1492, 1452 (C−H bending, backbone); 1600 (C═C stretching, aromatic); 758 and 700 (C−H bending, aromatic).

Poly(ethoxylated fluoroalkyl acrylate)-block-polystyrene (IV). One gram of poly(acrylic acid)-*block*-polystyrene (2.19 mmol acrylic acid) was dissolved in 5 mL of anhydrous pyridine. DCC (6.57 mmol), DMAP (0.823 mmol), and Zonyl FSO-100 (6 g) were dissolved in tetrahydrofuran and added dropwise to the polymer solution. The reaction mixture was stirred at room temperature for about 2.5 days. Dicyclohexylurea formed during the reaction was removed by filtration. After concentration under reduced pressure, the polymer solution was poured into excess methanol. Further purification was achieved by precipitating the polymer from tetrahydrofuran into methanol.

^{1}H NMR (300 MHz, $CDCl_3$, δ): 6.5 and 7.1 (5H, styrene); 4.16 (br s, 2H, −COOCH_2−); 3.77 (t, 2H, −COOCH_2CH_2−); 3.64 (br s, −OCH_2CH_2O−); 2.42 (m, 2H, −CH_2CF_2−); 1.86, 1.43 (backbone). ^{19}F NMR (282.24 MHz, $CDCl_3$, CF_3COOH reference, δ): −126.65, −124.16, −123.38, −122.41, −113.95, −81.27 (3F, −CF_3). IR (dry film) $\tilde{\nu}_{max}$ (cm^{-1}): 3026 (C−H stretching, aromatic); 2922 (C−H stretching, backbone); 1731 (C═O stretching, ester);

Scheme 1. Synthesis of Block Copolymers with Ethoxylated Fluoroalkyl Side Chains

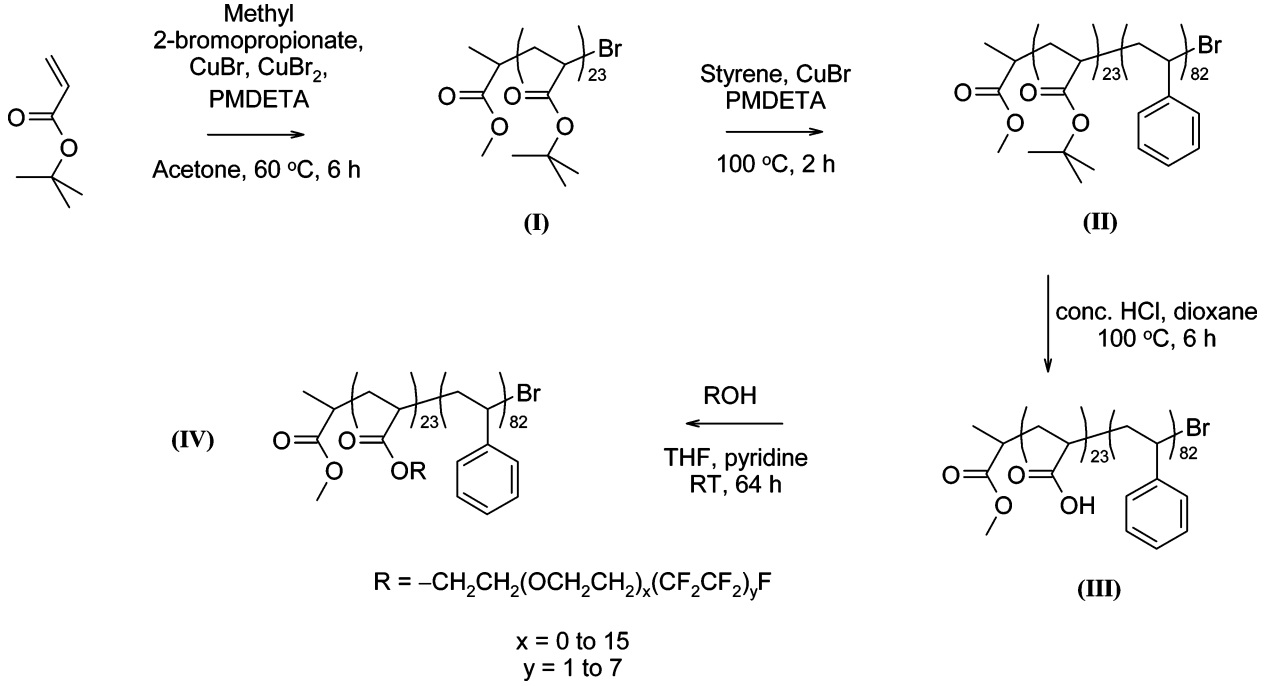

1490, 1450 (C−H bending, backbone); 1600 (C═C stretching, aromatic); 1400−1000 (C−F stretching); 754 and 698 (C−H bending, aromatic).

Gel permeation chromatography of a THF solution of polymers (1 mg/mL) was carried out using four Waters Styragel HT columns operating at 40 °C and Waters 490 ultraviolet (λ = 254 nm) and Waters 410 refractive index detectors. The molecular weight range of the columns was from 500 to 10^7 g/mol. THF was used as the eluent at a flow rate of 1 mL/min, and toluene was used as marker for flow calibration. The IR spectra of the polymers cast as films from THF solution on sodium chloride or potassium bromide salt plates were collected using a Mattson 2020 Galaxy Series FTIR spectrometer. ^{1}H and ^{19}F NMR spectra were recorded using a Varian Gemini spectrometer with deuterated solvents. Matrix-assisted laser desorption ionization time-of-flight (MALDI-TOF) mass spectroscopy of the ethoxylated fluoroalkyl surfactant was performed using an Applied Biosystems 4700 Proteomics Analyzer with 4-hydroxy-3,5-dimethoxycinnamic acid (CAS no. 530-59-6) as the matrix.

2.3. Surface Characterization. Samples for surface characterization were prepared by spin coating a 3% (w/v) chloroform solution of the amphiphilic block copolymer on silicon wafers using a Cee model 100CB spin coater at 2000 rpm (acceleration of 1000 rpm/s) for 30 s. The surfaces were dried in a low-vacuum oven at 60 °C for 12 h before further annealing at 120 or 150 °C in a high-vacuum oven. Test surfaces for biofouling assays were prepared on 3 in. × 1 in. glass microscope slides. The glass slides were cleaned in hot piranha solution (concentrated sulfuric acid + 30 wt % hydrogen peroxide solution, 7:3 v/v), rinsed with distilled water, and dried using nitrogen. A 2% (w/v) solution of (3-glycidoxypropyl)-trimethoxysilane in 95% ethanol (with pH adjusted between 4.5 and 5 using acetic acid) was prepared by adding the silane to the ethanol solution and stirring for 5 min. The glass slides were then soaked in this solution for at least 1 h, rinsed with ethanol, and heated in an oven at 110 °C for 10 min. The GPS-functionalized glass slides were spin coated with a toluene solution containing 5% (w/v) MA-SEBS and 2% (w/v) SEBS and annealed in a vacuum oven at 120 °C for 12 h. The styrene content of both SEBS and MA-SEBS was 30 wt %, and the latter had 1.4−2.0 wt % of grafted maleic anhydride. The maleic anhydride groups in the polymer backbone react with epoxy groups on the glass surface, improving the bonding of the coating to the glass. The surfaces were further spin coated three times with a 12% (w/v) solution of SEBS in toluene (2500 rpm) followed by vacuum annealing at 120 °C for 12 h. A 1.5% (w/v) solution of the amphiphilic block copolymer (1.5 g/100 mL of chloroform) was spray coated onto the SEBS surface using a Badger model 250 airbrush and 50 psi nitrogen gas to obtain a polymer surface density of 1.5 to 2 mg/cm^2. The surfaces were finally dried in a low-vacuum oven at 60 °C for 18 h (or 60 °C for 18 h and 120 °C for 6 h) to ensure the complete removal of solvents and to study the effect of annealing on antifouling properties. The fouling-release properties of surfaces prepared under two different annealing conditions were compared.

Contact angles were measured using an NRL contact angle goniometer (Ramé-Hart model 100-00) at room temperature. Dynamic water contact angle measurements were performed by the addition and retraction of a drop of water on the surface. The contact angle of an air bubble over the polymer surface immersed in water was determined using the captive bubble method.[29,30] An air bubble, which was snapped off of the tip of a 22 gauge stainless steel syringe needle (0.7 mm o.d. and 0.4 mm i.d.), was contacted by the surface immersed in water, and the contact angle was measured. The angles reported are those between the surfaces and the air bubble, measured on the water side. Thus, a low captive-bubble contact angle indicates a hydrophilic surface, while a higher angle indicates a more hydrophobic surface.

Surface roughness was determined using a 3-D interferometric noncontact surface profiler (ADE Phase-Shift MicroAXM-100HR). Root-mean-square (rms) roughness values were determined over regions of 631 μm × 849 μm size and averaged over at least 10 measurements. The surface morphology and surface roughness on a local scale were studied using a Veeco Dimension 3100 scanning probe microscope in tapping mode.

X-ray photoelectron spectroscopy (XPS) measurements were performed using an Axis Ultra XPS system (Kratos) with a monochromatic Al Kα X-ray source (1486.6 eV) operating at 225 W under 7.0×10^{-9} Torr vacuum. Charge compensation was carried out by injection of low-energy electrons into the magnetic lens of the electron spectrometer. The pass energy of the analyzer was set at 40 eV. The energy resolution was set at 0.1 eV with a dwell time of 500 ms. The spectra were analyzed using CasaXPS v. 2.1.9 software.

(29) Adamson, A. W. *Physical Chemistry of Surfaces*, 3rd ed.; Wiley: New York, 1976.

(30) Andrade, J. D.; King, R. N.; Gregonis, D. E.; Coleman, D. L. *J. Polym. Sci., Polym. Symp.* **1979**, *66*, 313−336.

NEXAFS experiments were carried out on the U7A NIST/Dow materials characterization end-station at the National Synchrotron Light Source at Brookhaven National Laboratory. The principles of NEXAFS and a description of the BNL beamline have been outlined elsewhere.[31,32] The NIST/Dow materials characterization end-station was equipped with a sample holder positioned on a goniometer, which controlled the orientation of the sample with respect to the polarization vector of the X-rays. The partial-electron-yield (PEY) signal was collected using a channeltron electron multiplier with an adjustable entrance grid bias (EGB). Unless specified, all of the data reported here are for a grid bias of −150 V. The channeltron PEY detector was positioned at an angle of 45° with respect to the incoming X-ray beam and in the equatorial plane of the sample chamber. To eliminate the effect of incident beam intensity fluctuations and monochromator absorption features, the PEY signals were normalized by the incident beam intensity obtained from the photoyield of a clean gold grid. A linear pre-edge baseline was subtracted from the normalized spectra, and the edge jump was arbitrarily set to unity at 320 eV, far above the edge, a procedure that enabled the comparison of different NEXAFS spectra for the same number of carbon atoms within the Auger electron sampling depth of the surface.[33] The photon energy was calibrated by adjusting the peak position of the lowest π^* phenyl resonance from polystyrene to 285.5 eV.[34] Each measurement was taken on a fresh spot on the sample in order to minimize possible beam damage effects.

2.4. Biofouling Assays. *Leaching.* Slides were incubated at about 20 °C for 3 days in a 30 L tank of recirculating deionized water. Equilibration with seawater was achieved by transferring the slides to dishes containing artificial seawater 1 h prior to the start of the experiment.

Settlement of Zoospores. Fertile plants of *Ulva linza* were collected from Wembury Beach, England (50°18′ N, 4°02′ W). Zoospores were released and prepared for attachment experiments as described previously.[35] Ten-milliliter portions of zoospore suspensions were pipetted into individual compartments of polystyrene culture dishes (Fisher), each containing a glass microscope slide. The dishes were incubated in the dark at about 20 °C. After 1 h, the slides were gently washed in seawater to remove zoospores that had not attached. The density of zoospores attached to the surface was counted on each of three replicate slides using an image analysis system attached to a fluorescence microscope. Spores were visualized by the autofluorescence of chlorophyll. Counts were made for 30 fields of view (each 0.17 mm^2) on each slide.

Growth of Sporelings. Spores were allowed to settle for 1 h in the dark. After washing, sporelings were cultured in an enriched seawater medium in individual (10 mL) wells in polystyrene dishes under illuminated conditions. The medium was refreshed every 2 days, and the sporelings were cultured for 8 days. The strength of attachment of the sporelings was assessed using a wall shear stress of 53 Pa in a turbulent flow channel.[15,36]

Sporeling biomass was determined in situ by measuring the fluorescence of the chlorophyll contained within the sporelings using a Tecan fluorescence plate reader. The biomass is quantified in terms of relative fluorescence units (RFU). The RFU value for each slide is the mean of 196 point fluorescence readings. The data are expressed as the mean RFU of six replicate slides; error bars show the standard error of the mean.

Navicula Settlement and Strength of Attachment. Navicula cultures were prepared as described in Holland et al.[17] Ten milliliters of the cell suspension was added to individual compartments of polystyrene culture dishes (Greiner Bio-1) each containing a glass microscope slide. After 2 h in the light at about 20 °C, the slides were very gently washed in seawater to remove cells that had not properly attached. The density of cells attached to the surface was counted on each slide using an image analysis system attached to a fluorescence microscope. Counts were made for 30 fields of view (each 0.17 mm^2) on each slide.

Slides settled with *Navicula* were exposed to shear stress in a water channel. The number of cells remaining attached was compared with unexposed control slides (used to determine settlement as above). Cells were counted using the image analysis system as described above.

Ulva and *Navicula* assays were performed on the spray-coated amphiphilic surfaces vacuum dried at 60 °C. In addition, surfaces annealed at 120 °C were also tested with *Ulva* to study the effect of annealing on antifouling properties. Acid-washed glass slides and glass slides coated with poly(dimethyl siloxane) were used as standards. The acid-washed glass slides were prepared by washing in Decon detergent before soaking in 1 M hydrochloric acid for 24 h. The PDMS surfaces were prepared using Silastic T-2 (Dow-Corning), as described in Hoipkemeier-Wilson et al.[8,37] Silastic T-2 was used because of its good dimensional stability, optical transparency, and minimal unknown or nondisclosed additives.[38] The base resin and curing agent were mixed in a 10:1 mass ratio as recommended by the manufacturer, applied to glass microscope slides functionalized with allyltrimethoxy silane (for covalently attaching the PDMS elastomer to the substrate), and cured by a platinum-catalyzed hydrosilylation reaction at 50 °C for 5 h. The Silastic T-2 mixture consisted of a vinyl-terminated dimethyl siloxane polymer ($H_2C{=}CH\{Si(CH_3)_2O\}_nSi(CH_3)_2CH{=}CH_2$, about 60 wt %) and filler silica particles modified with (trimethylsilyl)oxy ($(CH_3)_3SiO-$) groups (about 25 wt %) and (ethenyldimethylsilyl)-oxy ($H_2C{=}CH-Si(CH_3)_2O-$) groups (about 10 wt %). (Dimethylhydrogensilyl)oxy ($HSi(CH_3)_2O-$)-modified silica particles and vinyl-terminated methylvinyl siloxane oligomers ($H_2C{=}CH\{Si(CH_3)_2O\}_p\{Si(CH_3)(CH{=}CH_2)O\}_qSi(CH_3)_2CH{=}CH_2$) acted as cross linkers. The Silastic T-2 PDMS surface was included as a standard for the biofouling studies because its fouling-release efficacy has already been established against barnacle fouling[39] and in a number of laboratory studies using algae.[7,8,17,19]

3. Results and Discussion

3.1. Polymer Synthesis. Polymer analogous reactions have previously been used to prepare polymers with functional side chains. Wang et al.[40] have prepared block copolymers with semifluorinated side chains by introducing hydroxyl groups into the polyisoprene block of polystyrene-*block*-polyisoprene followed by esterification with semifluorinated carboxylic acids. Hourdet et al.[41] synthesized poly(acrylic acid)-*graft*-poly(ethylene glycol) by reacting ω-amino PEG with poly(acrylic acid). Poly(methacrylic acid)-*graft*-poly(ethylene glycol) has been similarly prepared by Poe et al.[42] The synthesis of polystyrene-*block*-

(31) Genzer, J.; Sivaniah, E.; Kramer, E. J.; Wang, J.; Korner, H.; Xiang. M.; Yang, S.; Ober, C. K.; Char, K.; Chaudhury, M. K.; Dekoven, B. M.; Bubeck, R. A.; Fisher, D. A.; Sambasivan, S. In *Applications of Synchrotron Radiation Techniques to Materials Science IV*, MRS Symposium Proceedings, San Francisco, CA, Apr 13−17, 1998; Mini, S. M., Perry, D. L., Stock, S. R., Terminello, L. J., Eds.; Materials Research Society: Warrendale, PA, 1998; Vol. 524, p 365.

(32) Genzer, J.; Sivaniah, E.; Kramer, E. J.; Wang, J.; Koerner, H.; Char, K.; Ober, C. K.; DeKoven, B. M.; Bubeck, R. A.; Fischer, D. A.; Sambasivan, S. *Langmuir* **2000**, *16*, 1993−1997.

(33) Samant, M. G.; Stöhr, J.; Brown, H. R.; Russell, T. P.; Sands, J. M.; Kumar, S. K. *Macromolecules* **1996**, *29*, 8334−8342.

(34) Liu, Y.; Russell, T. P.; Samant, M. G.; Stöhr, J.; Brown, H. R.; Cossy-Favre, A.; Diaz, J. *Macromolecules* **1997**, *30*, 7768−7771.

(35) Callow, M. E.; Callow, J. A.; Pickett-Heaps, J.; Wetherbee, R. *J. Phycol.* **1997**, *33*, 938−947.

(36) Schultz, M. P.; Finlay, J. A.; Callow, M. E.; Callow, J. A. *Biofouling* **2000**, *15*, 243−251.

(37) Additional information is available on the Internet at http://www.dowcorning.com in the documents titled "Silastic T-2 Translucent Base and Silastic T-2/T-2 Durometer Curing Agent" (reference number 80-3143-01) and "Mold Making Products For Industrial Applications" (reference number 10-1258D-01). Surface characterization and mechanical properties of this coating are discussed in ref 38.

(38) Feinberg, A. W.; Gibson, A. L.; Wilkerson, W. R.; Seegert, C. A.; Wilson, L. H.; Zhao, L. C.; Baney, R. H.; Callow, J. A.; Callow, M. E.; Brennan, A. B. In *Syntheis and Properties of Silicones and Silicone-Modified Materials;* Clarson, S. J., Fitzgerald, J. J., Owen, M. J., Smith, S. D., Van Dyke, M. E., Eds.; ACS Symposium Series 838; American Chemical Society: Washington DC, 2003; pp 196−211.

(39) Sun, Y.; Guo, S.; Walker, G. C.; Kavanagh, C. J.; Swain, G. W. *Biofouling* **2004**, *20*, 279−289.

(40) Wang, J.; Mao, G.; Ober, C. K.; Kramer, E. J. *Macromolecules* **1997**, *30*, 1906−1914.

(41) Hourdet, D.; L'Alloret, F.; Audebert, R. *Polymer* **1997**, *38*, 2535−2547.

poly(*tert*-butyl acrylate) used in this work was based on a procedure reported by Davis and Matyjaszewski.[43] The *t*BA block was quantitatively hydrolyzed to acrylic acid using concentrated HCl. Esterification at room temperature using DCC and DMAP resulted in a high degree of attachment of the fluorinated PEG (Zonyl FSO-100) to the acrylic acid backbone. The extent of attachment, calculated from the ratios of $-COOCH_2CH_2-$ protons of the side chains and the aromatic protons of styrene, was at least 95%.

3.2. Molecular Weight, Its Distribution, and Block Copolymer Composition. The GPC molecular weight distributions of poly(*t*BA), poly(*t*BA)-*block*-PS, and the block copolymer with ethoxylated fluoroalkyl side chains showed that all of the polymers had a relatively narrow polydispersity index. The GPC elution curves are shown in the Supporting Information section. The degree of polymerization of the *t*BA block, determined by ^{1}H NMR using the backbone $>CH-$ and terminal $>CH-$Br peaks, was found to be 23. Using the protons attached to the aromatic ring of styrene and all of the protons in the block copolymer, the mole percent of styrene units in the polymer was determined to be 78%. Thus, the degree of polymerization of the polystyrene block is about 82. The molecular weight of the PS block (about 8500 g/mol) is close to that of the PS blocks in SEBS.

The fluorinated PEG, $F(CF_2CF_2)_y(CH_2CH_2O)_xCH_2CH_2OH$, used for attachment has a broad distribution of molecular weights, with $x = 0-15$ and $y = 1-7$ specified by the supplier. MALDI-TOF spectroscopy showed two species with mass-to-charge ratios of 695.25 g/mol ($y = 5$, $x = 3$) and 739.28 g/mol ($y = 5$, $x = 4$) as the major components. Molecules with $y = 5$, $x = 5, 6$ and $y = 2$, $x = 6-12$ could also be identified as other components in the mixture (cf. Supporting Information). On the basis of the areas of $-CF_2CH_2-$ protons and $-CF_3$ fluorines in ^{1}H and ^{19}F NMR spectra, respectively, the average composition was determined to be $y = 3.4 \pm 0.7$ and $x = 5.9 \pm 1.0$. After reaction with polystyrene-*block*-poly(acrylic acid), the average composition of the side chain, determined by NMR spectroscopy, was $y = 3.0 \pm 0.7$ and $x = 3.5 \pm 0.6$.

3.3. Water Contact Angle Measurements. A 3% (w/v) chloroform solution of the block copolymer with ethoxylated fluoroalkyl side chains was spin coated onto a silicon wafer and vacuum dried at 60 °C for 24 h. The advancing and receding water contact angles were determined to be (94 ± 1) and (34 ± 1)°, respectively. The contact angle of an air bubble on the surface immersed in water decreased from (55 ± 2)° immediately after immersion to (46 ± 2)° after a day and (41 ± 2)° after 3 days and reached an equilibrium value of (31 ± 2)° after 2 weeks. The decrease in the contact angle is attributed to the migration of the PEG segments to the water−polymer interface. Such a molecular reorganization of the surface can occur by (i) the migration of the polystyrene block away from the interface and (ii) the reorientation of the side chains by the mechanism proposed in Figure 2. In the latter case, the flipping of the side chains would facilitate the enthalpically favorable interaction of PEG with water while simultaneously minimizing the water contact of the hydrophobic fluoroalkyl segments. The equilibrium surface structure, from the point of view of the minimization of enthalpy, would be one in which the polystyrene block and the fluoroalkyl segments are completely buried under the PEG groups. That the actual surface morphology is close to the expected picture is corroborated by the equilibrium value of the captive-bubble contact angle (~31°), which is similar to that for surface-tethered PEGylated polymer brushes in contact with water.[44] The advancing and receding water contact angle measurements in air indicate that the molecular reorganization occurs on a short time scale (corresponding to the rate of addition and retraction of the water drop). These measurements possibly reflect the molecular reorganization by the flipping of the side chains. On the contrary, the captive-air-bubble contact angle measurements indicate surface reconstruction over a period of days. This slower reconstruction is attributed to the migration of the polystyrene block away from the surface and the fluorinated block toward the surface.

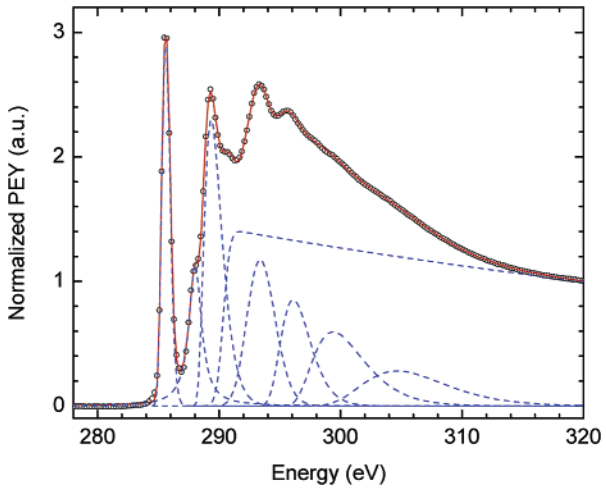

Figure 3. NEXAFS spectrum of a spin-coated surface of amphiphilic polymer on a silicon wafer after annealing at 120 °C for 12 h. Circles are experimental data points, the solid line is the best-fit curve, and the curves with dotted lines are deconvoluted peaks.

The underwater octane contact angle, the angle between the surface and an octane drop measured on the water side, was (55 ± 3)°. From the captive air bubble and octane drop contact angles, the polymer−water interfacial energy could be estimated[30] to be about 4 mJ/m^2, a fairly low value as would be expected for a hydrated PEGylated surface. The advancing and receding water contact angles on the spray-coated amphiphilic surfaces with SEBS bottom layers were (97 ± 3) and (42 ± 5)° with no significant difference between surfaces annealed at 60 and 120 °C.

3.4. Near-Edge X-ray Absorption Fine Structure Spectroscopy. Figure 3 shows the NEXAFS spectrum of a surface prepared by spin coating a 3% (w/v) solution of the amphiphilic block copolymer in chloroform. After drying in a vacuum oven at 60 °C, the surface was further annealed at 120 °C for 12 h. The NEXAFS spectrum was obtained at an X-ray incidence of 55° to the surface normal. The entrance grid bias of the channeltron PEY detector was −150 V. The experimental spectrum was deconvoluted by performing a nonlinear least-squares fit using a series of Gaussian peaks for resonances corresponding to bound-state transitions and a Gaussian step multiplied by an exponential decay for the continuum step.[45] Peak assignments were made on the basis of calibrated NEXAFS spectra of polystyrene,[34] poly(ethylene oxide),[46] and poly(methyl methacrylate)[46] reported in the literature. The phenyl ring C 1s → $\pi^*_{C=C}$ resonance occurs at 285.5 eV. The resonance at 287.7 eV is due to the 1s → σ^*_{C-H}

(42) Poe, G. D.; Jarrett, W. L.; Scales, C. W.; McCormick, C. L. *Macromolecules* **2004**, *37*, 2603−2612.

(43) Davis, K. A.; Matyjaszewski, K. *Macromolecules* **2001**, *34*, 2101−2107.

(44) Andruzzi, L.; Senaratne, W.; Hexemer, A.; Sheets, E. D.; Ilic, B.; Kramer, E. J.; Baird, B.; Ober, C. K. *Langmuir* **2005**, *21*, 2495−2504.

(45) Stöhr, J. *NEXAFS Spectroscopy*; Springer-Verlag: New York, 1996; Chapter 7, p 211.

(46) Kikuma, J.; Tonner, B. P. *J. Electron Spectrosc. Relat. Phenom.* **1996**, *82*, 53−60. The excitation energies reported in this paper must be adjusted by 0.6 eV for comparison with our values. The $\pi^*_{C=C}$ resonance has been calibrated to 284.9 eV here.

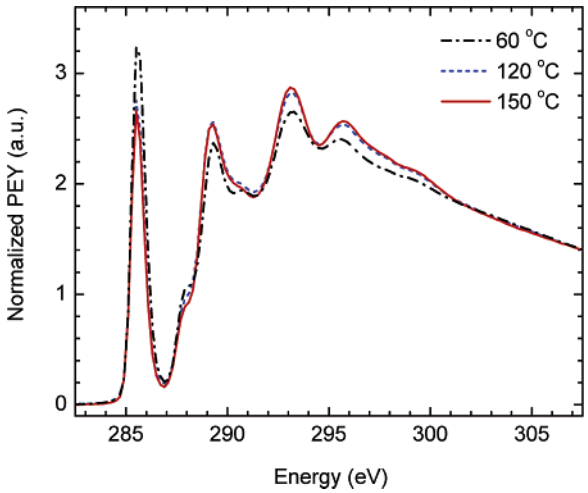

Figure 4. NEXAFS spectra at an X-ray incident angle of 55° with respect to the normal of surfaces prepared by spin coating a 3% (w/v) solution of the block copolymer in chloroform and (a) vacuum drying at 60 °C for 12 h, followed by annealing at (b) 120 °C for 12 h and (c) 150 °C for 12 h.

transitions. The peak at 289 eV is attributed to 1s → $\pi^*_{C=O}$ resonance whereas that at 299 eV is probably a C═O σ^* resonance. The σ^*_{C-F}, σ^*_{C-O}, and σ^*_{C-C} transitions, corresponding to the amphiphilic side chains, result in the peaks at 293 and 295.8 eV. The continuum step was found to be located near 290 eV. The intensity of the 1s → σ^*_{C-F} peak at 293 eV shows a weak, nonmonotonic relationship when plotted against $\sin^2\theta$, where θ is the X-ray angle of incidence,[33] indicating that the fluoroalkyl tail of the ethoxylated fluoroalkyl side chains are unoriented with respect to the surface normal. Unlike polymers with long semifluorinated alkyl side chains,[40] the ethoxylated fluoroalkyl side chains thus appear not to form a smectic liquid-crystalline phase. The lack of liquid crystallinity was also evident from the absence of melting peaks in differential scanning calorimetry (DSC) of the block copolymer. This may be due to the polydispersity of the ethoxylated fluoroalkyl side chains. Zonyl FSO-100 has a broad distribution of perfluoroethylene and ethoxy group lengths. The difference in the lengths of the poly(ethylene oxide) spacer is expected to hinder liquid crystalline packing of the fluoroalkyl tails.

Effect of Annealing Temperature. Figure 4 shows the NEXAFS spectra of surfaces annealed at three different temperatures. Two observations are noteworthy. First, the intensity of the C═C π^* peak corresponding to the polystyrene block is lower when the surface is annealed at 120 or 150 °C compared to 60 °C. Second, the intensity of the C−F σ^* resonance increases with annealing. This result is an indication of the preferential segregation of the amphiphilic block to the air−polymer interface and suggests that the amphiphilic block has a lower surface energy than polystyrene, despite the presence of the higher-energy PEG moieties. This can be attributed to the diblock nature of the side chains and the tendency of the fluoroalkyl groups to be selectively present at the air−polymer interface. The low-surface-energy fluoroalkyl groups seem to compensate for the higher-surface-energy PEG moieties. Similar anchoring of a high-surface-energy group at the air−polymer interface by a covalently attached low-surface-energy group has been observed by Thanawala and Chaudhury[47] and Vaidya and Chaudhury.[27] XPS spectra of these surfaces, discussed in the next section, also confirmed the NEXAFS results.

(47) Thanawala, S. K.; Chaudhury, M. K. *Langmuir* **2000**, *16*, 1256−1260.

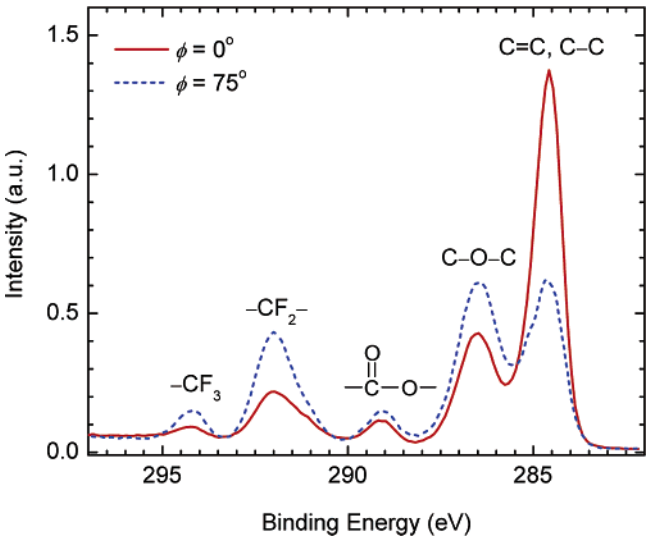

Figure 5. Area-normalized XPS spectra, at two different emission angles, of the amphiphilic block copolymer spin coated onto silicon and annealed at 120 °C for 12 h. The emission angle, ϕ, is the angle made by the surface normal with the escape path of electrons emitted by the surface.

3.5. Variation of Surface Composition with Depth. NEXAFS spectroscopy indicated a preferential segregation of the amphiphilic block to the air−polymer interface, an observation consistent with expectations from a mixture of molecules with significantly different surface energies. Polystyrene has a surface energy of 39.3 mJ/m^2, and poly(ethylene oxide) has a higher surface energy of 43 mJ/m^2. A surface completely covered by fluoroalkyl groups has a surface energy as low as 8 mJ/m^2.[40] The surface segregation of the amphiphilic block should result in a depth-dependent concentration profile, which was investigated using two techniques: angle-resolved XPS and depth profiling using NEXAFS.

Figure 5 shows the XPS spectra of the block copolymer film coated on silicon, obtained at two different electron emission angles, ϕ. The electron emission angle, ϕ, is the angle between the surface normal and the path taken by the electrons toward the detector. The sampling depth, d, is approximately $\lambda \cos\phi$, where λ is the inelastic mean free path (IMFP). The electron IMFP for the polymer with structure shown in Figure 1 can be estimated using the quantitative structure−property approach of Cumpson,[48] based on the zeroth-order valence connectivity indices of Kier−Hall, to be

$$\lambda^{1\ \mathrm{keV}} = \frac{31.17\{4.671m + (4.393 + 1.822x + 2.512y)n\} + 4.207m}{8m + (8 + 3x + 6y)n} + 11.04\ \text{Å} \quad (1)$$

where the superscript 1 keV indicates that the estimated IMFP is for electrons with an energy of 1 keV. The IMFP for an electron with energy E (keV) can be obtained using[48,49]

$$\lambda = \lambda^{1\ \mathrm{keV}}(E/\mathrm{keV})^{0.79} \quad (2)$$

(48) Cumpson, P. J. *Surf. Interface Anal.* **2001**, *31*, 23−34.

(49) Equation 1 assumes a statistically homogeneous mixture of the two monomers in the block copolymer thin film, despite the block architecture of the copolymer and the experimentally observed fact that there is segregation of the amphiphilic block to the surface (cf. Figure 5). However, the $\lambda^{1\ \mathrm{keV}}$ values for the PS and the amphiphilic blocks (calculated separately) were 29.8 and 26.8 Å (for $x = 4$, $y = 3$), respectively, and within ±11% of each other, making eq 1 a reasonable approximation for IMFP of electrons emitted by the block copolymer.

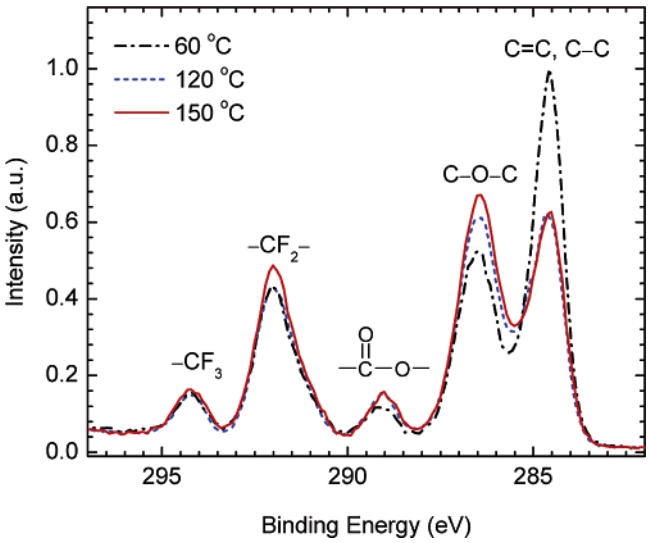

Figure 6. Area-normalized XPS spectra of surfaces prepared by spin coating a 3% (w/v) solution of the block copolymer in chloroform and (a) vacuum drying at 60 °C for 12 h, followed by annealing at (b) 120 °C for 12 h and (c) 150 °C for 12 h. An electron emission angle of 75° was used.

Thus, the inelastic mean free path for a C 1s electron with a binding energy of 294 eV,[50] and hence a kinetic energy of 1192.6 eV, is about 3.2 nm. For electron emission along the surface normal, more than 63% of the photoelectrons originating from depths below λ (3.2 nm) would have lost energy by inelastic scattering. These inelastically scattered electrons will not contribute to peak intensities in which we are interested. In other words, most of the electrons detected (using $\phi = 0°$) are from within a depth of λ below the surface. The sampling depth using an emission angle of 75° will be 25.8% of that using 0° emission, making the XPS results at this angle sensitive primarily to the chemical bonding within about 1 nm of the surface.

It is seen from Figure 5 that the peak at 284.6 eV due in part to polystyrene decreases and the peaks corresponding to the amphiphilic side chains, at 294 eV from $-CF_3$, 292 eV from $-CF_2-$, and 286.6 eV from $-CH_2CH_2O-$, increase as the sampling depth is decreased. This indicates the presence of a thin layer of ethoxylated fluoroalkyl groups at the surface as well as a higher concentration of C atoms not bonded to F or O in a layer below the surface. Logically, this subsurface layer contains phenyl rings from PS that XPS cannot distinguish from the C atoms in the polymer backbone within the peak centered at 284.6 eV. However, detailed analysis of the peak shape shows a small "shake up" peak from the PS phenyl rings centered at about 291.2 that accounts for the asymmetry of the $-CF_2-$ peak at 292 eV in Figure 5.

Figure 6 shows the XPS spectra of surfaces annealed at 60, 120, and 150 °C, determined using an electron emission angle of 75°. The results show a progressive depletion of C atoms not bonded to F or O and an enrichment of $-CF_2-$, $-CH_2CH_2O-$, and $-COO-$ carbon atoms of the amphiphilic side chains as the annealing temperature is increased. This is evident from the intensity of the peaks at 284.6 and 286.6 eV, associated with C═C carbon atoms of styrene and $-CH_2CH_2O-$ carbon atoms of PEG, respectively, and is consistent with inferences from NEXAFS spectroscopy (cf. Figure 4). Surface reconstruction occurs on annealing where the thin layer of amphiphilic side chains is further enriched in the fluoroalkyl and PEG components, possibly by migration of the higher-surface-energy PS block toward the bulk.

Depth Profiling Using NEXAFS Spectroscopy. Although XPS is not capable of separating C atoms in polystyrene phenyl rings from C atoms in the polymer backbone, NEXAFS spectroscopy can directly monitor the former from the sharp 1s $\rightarrow \pi^*_{C=C}$ resonance at about 285.5 eV. Depth profiling using NEXAFS peaks can be accomplished by two methods. The first method is based on making the entrance grid bias (EGB) of the channeltron photoelectron detector progressively more negative so that only Auger electrons originating from increasingly thinner sample depths and carrying information about the molecular composition of the film could be detected.[51] The second method involves obtaining the NEXAFS spectra at different electron emission angles by rotation of the sample (about a vertical axis) relative to the "in-plane"[52] partial electron yield (PEY) detector, as shown in Figure 7. Results from the second method will be described in this section.

Figure 8 shows the experimental variation in the normalized partial electron yields at 285.5 and 293.0 eV, corresponding to transitions to $\pi^*_{C=C}$ and σ^*_{C-F} orbitals, respectively, with the cosine of the emission angle, ϕ. As discussed in the previous section, the sampling depth, d, at an emission angle, ϕ, is proportional to $\lambda \cos \phi$, thus making the abscissa of Figure 8

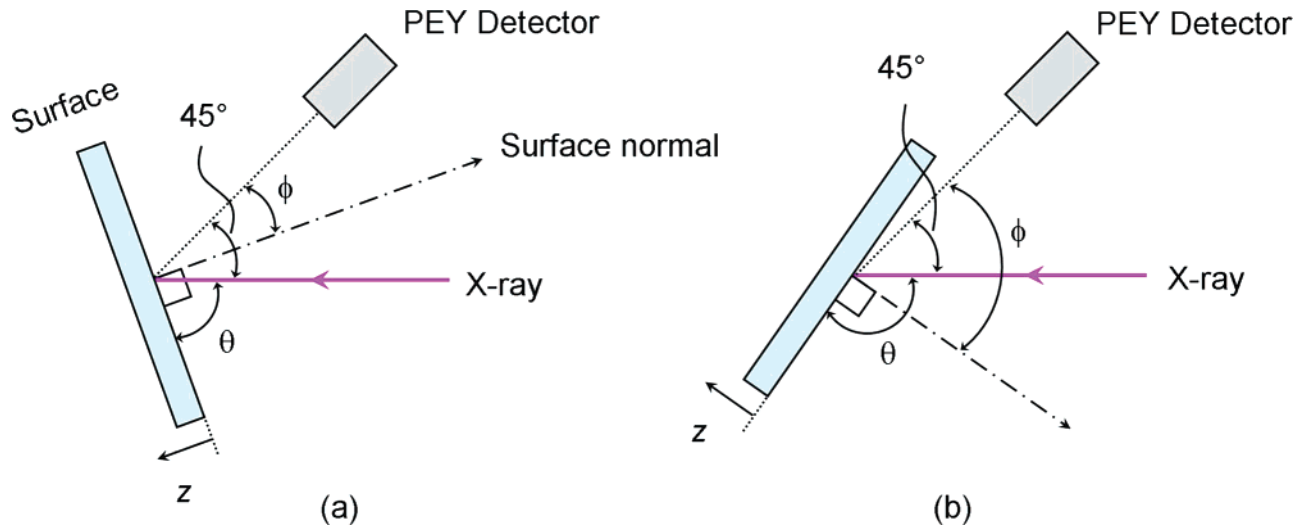

Figure 7. Experimental arrangement for NEXAFS depth-profiling experiments (top view). The electron emission angle, ϕ, is varied by rotating the surface about an axis normal to the plane of the paper as shown in the two different configurations (a and b). The angle between the path of the incident X-ray photons and the emitted Auger electrons is fixed and is about 45°.

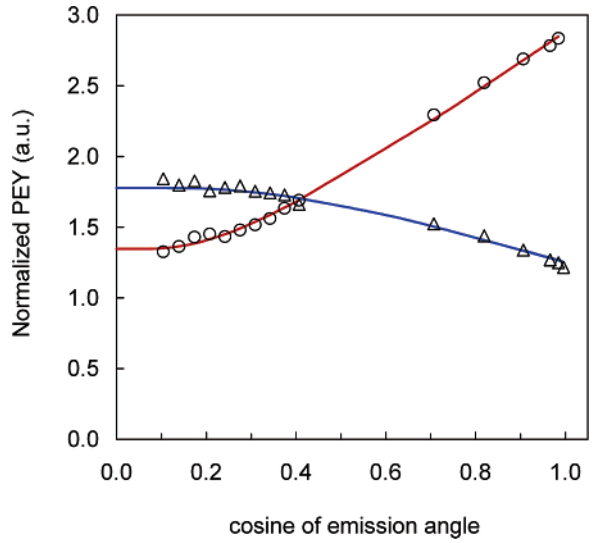

Figure 8. Experimental dependence of the PEY corresponding to 1s → $\pi^*_{C=C}$ resonance (○) and 1s → σ^*_{C-F} resonance (△) with the cosine of the electron emission angle, ϕ. The $\pi^*_{C=C}$ peak is associated with the phenyl ring C atoms whereas the σ^*_{C-F} signal arises from the C atoms bonded to F. The curves are theoretical fits assuming the model shown in eq 4.

directly proportional to the sampling depth. The smooth curves were obtained by fitting the experimental data with eq 3, which translates to the concentration profile $f(z)$ given in eq 4. Equation 3 was derived by first assuming a concentration profile, $f(z)$ (eq 4) and then using the equation relating the normalized PEY to the concentration profile of the phenyl ring C atoms (eq 7 discussed in the Appendix). In eqs 3 and 4, I_a is the normalized PEY of the $\pi^*_{C=C}$ resonance, $\sigma_x(h\nu)$ is the X-ray absorption cross section for photons of energy $h\nu$, z is the depth below the surface of the polymer film, and $f(z)$ is the fraction of the total number of C atoms, at depth z, that belong to the phenyl ring. The parameters b, m, and a of the model for $f(z)$ are positive numbers. It is seen that except at high electron emission angles (low values of cos ϕ) the assumed concentration profile fits the experimental data fairly well.

$$I_a = \frac{\sigma_x(285.5\text{ eV})}{\sigma_x(320.0\text{ eV})}\left\{b \pm m\lambda\cos\phi\exp\left(-\frac{a}{\lambda\cos\phi}\right)\right\} \quad (3)$$

$$f(z) = \begin{cases} b & 0 \le z \le a \\ b + m(z-a) & z > a \end{cases} \quad (4)$$

Figure 9 shows the fraction of C atoms that belong to the phenyl ring at different depths, z (nondimensionalized using λ), below the surface. It is seen that the polystyrene concentration is lower at the surface, shows little or no variation up to z/λ of about 0.4, and then increases deeper into the film. The actual depths, calculated using the value of 2.43 nm for λ, are also shown in Figure 9. A discussion on the selection of this value for λ is presented in the Appendix. In conjunction with results from angle-resolved XPS, one can conclude that the thin layer at the surface with a thickness of about 1.0 nm (corresponding to $z/\lambda = 0.4$), which is depleted in polystyrene, is occupied by the ethoxylated

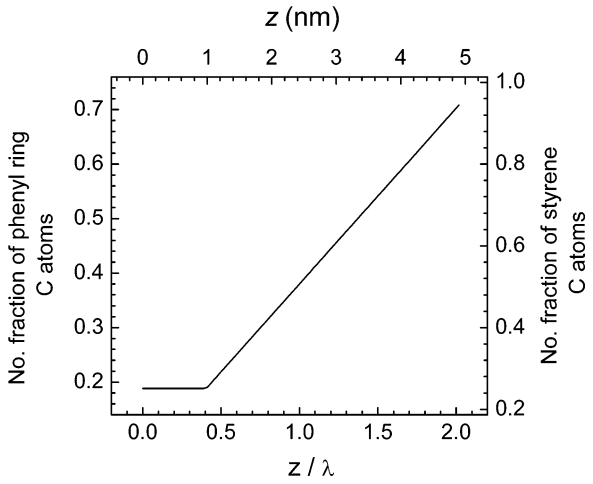

Figure 9. Variation of phenyl ring composition with depth z. The number fraction of C atoms in phenyl rings is equal to the number fraction of C atoms in polystyrene multiplied by 0.75. The top axis shows depth z normalized using an escape depth, λ, of 2.43 nm.

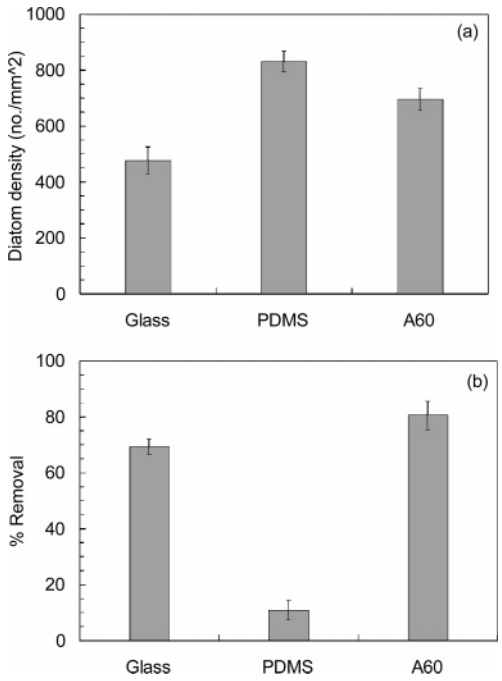

Figure 10. (a) Settlement and (b) percent removal of *Navicula* on glass, PDMS, and amphiphilic polymer surfaces. Each point represents the mean percentage removal from 90 counts from 3 replicate slides. Bars represent 95% confidence limits derived from arcsine-transformed data. A60 denotes the amphiphilic polymer surfaces annealed at 60 °C.

fluoroalkyl side chains at concentrations much higher than the average composition in the bulk.

In summary, XPS and NEXAFS results indicated the presence of the amphiphilic ethoxylated fluoroalkyl groups at the air−polymer interface. On immersing the surface in water, surface reconstruction occurred where the poly(ethylene glycol) parts of the ethoxylated fluoroalkyl side chains were exposed at the water−polymer interface. This is supported by water contact angle measurements for the surface in air, where the higher advancing water contact angle can be attributed to the presence of hydrophobic fluoroalkyl groups at the surface and the lower receding angle can be attributed to the presence of hydrophilic PEG. Contact angle measurements also suggested that surface reconstruction upon immersion in water occurred by two different mechanisms. The faster process is possibly due to reorientation

(50) The electrons originating from $-CF_3$ have the lowest kinetic energy in the C 1s spectrum of the amphiphilic polymer surface. These electrons have a higher probability of losing energy because of inelastic processes.

(51) Genzer, J.; Kramer, E. J.; Fischer, D. A. *J. Appl. Phys.* **2002**, *92*, 7070−7079.

(52) Fischer, D. A.; Colbert, J.; Gland, J. L. *Rev. Sci. Instrum.* **1989**, *60*, 1596−1602.

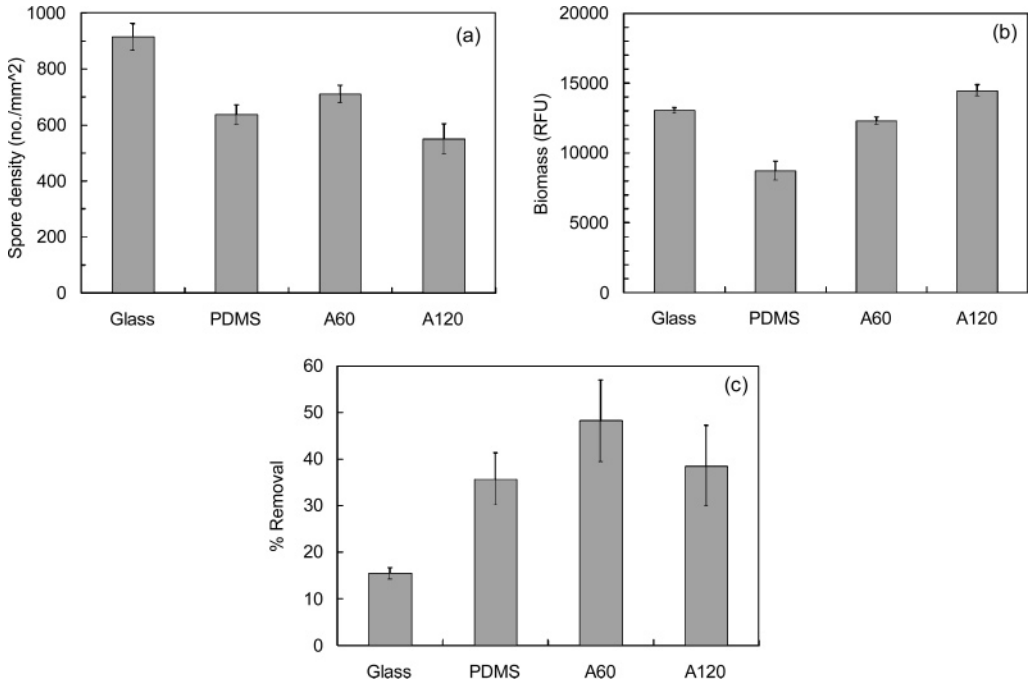

Figure 11. Settlement of *Ulva* spores on amphiphilic surfaces. Bars show 95% confidence limits from 90 counts, 30 on each of 3 replicate slides. (b) The growth of *Ulva* sporelings on amphiphilic surfaces after 7 days. Each point is the mean biomass from six replicate slides measured using a fluorescence plate reader (RFU; relative fluorescence unit). Bars show the standard error of the mean. (c) Percentage removal of *Ulva* sporelings from amphiphilic surfaces after exposure to a shear stress of 53 Pa in a water channel. Each point is the mean biomass from six replicate slides. Bars show the standard error of the mean derived from arcsine-transformed data. A60 and A120 are the amphiphilic surfaces annealed at 60 and 120 °C, respectively.

of the side chains as shown in Figure 2, whereas the slower process is that of diffusion of the polystyrene block toward the interior of the polymer coating and the surface-active block toward the polymer−water interface. The thermodynamically favored surface composition is expected to be the one that is rich in PEG groups. The associated minimization of polymer−water interfacial energy is expected to lower the driving force for adsorption of biomacromolecules at the surface.[27]

3.6. Surface Morphology. Scanning force microscopy of the spray-coated surfaces indicated a relatively uncomplicated surface morphology (cf. ref 28) and complete coverage of the underlying SEBS layer. The spray-coated surfaces used for the biofouling assays had a surface roughness of about 0.9 μm (determined over an area of 0.6 mm × 0.8 mm). The height profile of this surface, determined by optical interferometry, is available in the Supporting Information section. Spin-coated surfaces used for NEXAFS and XPS studies showed less than 3 nm surface roughness over 0.6 mm × 0.8 mm regions.

3.7. Marine Antifouling Properties. *Attachment of Diatoms.* The settlement densities of *Navicula* on glass, PDMS, and amphiphilic surfaces are shown in Figure 10a. Because the settlement of *Navicula* is by gravity, one would expect the same settlement density on all three surfaces. However, there were more cells adhered to the PDMS than to the glass standard surfaces, which probably reflects the weak attachment strength of *Navicula* to glass and the detachment of some cells at the gentle washing stage. This is confirmed from the data in Figure 10b, where the settled cells were exposed to 53 Pa wall shear stress in a turbulent flow channel and the percentages of removed cells are compared. The attachment strength was the lowest on the amphiphilic surface with (81 ± 5)% removal compared to (69 ± 3)% from glass and (11 ± 4)% from PDMS.

Settlement of Ulva Zoospores. Amphiphilic surfaces annealed at 60 and 120 °C were studied. The settlement density of spores was broadly similar on both of the amphiphilic surfaces and on the PDMS coatings (cf. Figure 11a). The settlement density on glass was higher.

Growth of Sporelings. Sporeling growth was also similar on all surfaces (cf. Figure 11b). There were no signs of toxicity from any of the surfaces.

Strength of Attachment of Sporelings. Removal of sporelings (cf. Figure 11c) from both amphiphilic surfaces was not statistically different to that from the PDMS standard, but removal from all three surfaces was significantly higher than from glass ($F_{3,20} = 7.18$, $P < 0.05$). It is likely that H bonding or electrostatic interactions[53] with glass caused stronger adhesion. In a different experiment, the 60 °C annealed surfaces were treated with spore suspensions of different concentrations, and the settled spores were cultured over a period of 8 days to form biofilms of sporelings. Sporeling removal was found to be greatest from surfaces that were exposed to the most concentrated spore suspension (and hence developed the highest sporeling density). We observed that whereas there was almost complete removal from the amphiphilic surface a large percentage of the sporelings remained on the glass surface even after exposure to water flow (cf. Supporting Information). Removal of sporelings from the amphiphilic surfaces seemed to be due to the entry of water between the sporeling biofilm and the coating. In other words, the sporelings were more strongly attached to each other than to the coating, and the biofilm detached in sheets.

As discussed in section 3.4, XPS and NEXAFS spectroscopy showed that the surface annealed at 120 °C had a lower content of polystyrene and a higher content of amphiphilic side chains than the surface annealed at 60 °C. However, the annealing temperature did not have a statistically significant effect on the release of sporelings. On the basis of the results of the captive-air-bubble contact-angle study, it seems that both the surfaces

(53) Roth, C. M.; Sader, J. E.; Lenhoff, A. M. *J. Colloid Interface Sci.* **1998**, *203*, 218−221.

(A60 and A120 in Figure 11) undergo surface reconstruction under water to result in surfaces predominantly covered by PEG, with the fluoroalkyl and styrene groups buried below. Thus, annealing did not have a significant effect on the adhesion strength of sporelings possibly because of similar molecular compositions and orientations at the polymer−water interface.

4. Conclusions

Surfaces of the comblike block copolymers with ethoxylated fluoroalkyl side chains are unique because they showed a high removal of both *Ulva* and *Navicula*. The PDMS surfaces resulted in a high release of *Ulva* sporelings, compared to a low release of diatom cells. The high removal of *Navicula* from the amphiphilic surface can be explained on the basis of the fact that the surface reconstructs to become as hydrophilic as a PEGylated surface when immersed in water and that *Navicula* adheres weakly to hydrophilic surfaces.[5,17] The settlement of *Ulva* spores on the amphiphilic surfaces is similar to that on PDMS. Similarly, the strengths of attachment of *Ulva* sporelings to the amphiphilic surfaces and PDMS are comparable. This may lead us to conclude that the surface becomes hydrophobic by exposing the fluoroalkyl groups when in contact with *Ulva*. However, the entrance of water between the *Ulva* biofilm and the coating surface suggests that the surface retained its hydrophilic character even after contact with the spore adhesive. The ingress of water between the coating and the biofilm was a distinctive property of the amphiphilic surfaces and was not observed in the case of PDMS or glass. Current knowledge on the chemistry of *Ulva* spore adhesive and its curing characteristics is insufficient to ascribe a mechanism for the detachment of sporelings from the amphiphilic coatings. Nevertheless, it is likely that the chemical ambiguity of the amphiphilic surface lowers the entropic and enthalpic driving forces[54] for the adsorption of adhesive macromolecules and hence the adhesion strength of the whole cell.

Acknowledgment. This research was supported by Office of Naval Research grants N00014-02-1-0170 to C.K.O. and E.J.K. and N00014-02-1-0521 to J.A.C. and M.E.C. Both grants are gratefully acknowledged. Additional funding came from the National Science Foundation Division of Materials Research (grant nos. DMR-0307233 and DMR-0208825) and from National Science Foundation Graduate Fellowship to K.E.S. It made use of the Hudson Mesoscale Processing, Polymer Characterization and Surface Imaging facilities of the Cornell Center for Materials Research (CCMR) and the Microscopy and Microanalysis Central Facility of the Materials Research Laboratory at UCSB, both with support from the National Science Foundation Materials Research Science and Engineering Centers (MRSEC) program (DMR-0079992 and DMR-0520415, respectively). The NEXAFS experiments were done at the National Synchrotron Light Source at Brookhaven National Laboratory, which is supported by the U.S. Department of Energy, Division of Materials Science and Division of Chemical Sciences. The PDMS surfaces (glass slides coated with T2 Silastic) were provided by Professor A. B. Brennan of the University of Florida. Dr. Dale Handlin of Kraton Polymers provided the SEBS elastomers.

Appendix

Relation between the Normalized Partial Electron Yield and the Concentration Profile of C Atoms Resulting in the π^* Resonance in NEXAFS Spectroscopy. The normalized PEY of Auger electrons resulting from the C 1s to $\pi^*_{C=C}$ transition, I_a (285.5 eV), can be expressed by the equation

$$I_a(285.5\text{ eV}) = \frac{\int_0^\infty I_0 A_0 \sigma_x(285.5\text{ eV})\rho_{C=C}(z)\omega_a \exp\left\{-\frac{z}{\lambda(285.5\text{ eV})\cos\phi}\right\} dz}{\sum_i \int_0^\infty I_0 A_0 \sigma_{x,i}(320.0\text{ eV})\rho_i(z)\omega_a \exp\left\{-\frac{z}{\lambda_i(320.0\text{ eV})\cos\phi}\right\} dz} \quad (5)$$

where I_0 (photons s^{-1} cm^{-2}) is the flux of incident X-ray photons; A_0 (cm^2) is the sample area exposed to the X-ray beam; $\sigma_x(h\nu)$ is the X-ray absorption cross section that depends on the photon flux and the probability of electron transition from the 1s shell to σ^*, π^*, or a continuum[55] final state; ρ (atoms/cm^2) is the area density of C atoms involved in a chemical bond of type i, for example, C═C, C−F, C−C, C−O, or C═O; z is the sample depth below the surface; $\lambda(h\nu)$ is the inelastic mean free path of Auger electrons resulting from X-ray photons with energy $h\nu$; and ω_a is the electron yield of the core excitation process. In eq 5, we have assumed that the fraction of X-ray photons absorbed in the top few nanometers of the film is small so that intensity variation with depth is not significant. It is seen that normalization of the measured PEY signal, as carried out in eq 5, accounts for the variations of I_0 and A_0 with the angle of X-ray incidence because these cancel out from the numerator and denominator of eq 5. The mean free path, λ, is not expected to vary significantly with the photon energy, $h\nu$, because the electrons detected are those emitted by an Auger mechanism. Furthermore, if the dependence of the X-ray absorption cross section, $\sigma_{x,i}$, on the final state of electronic transition of the C 1s electrons is neglected[56] and only its dependence on the photon energy is considered, then the above equation simplifies to

$$I_a(285.5\text{ eV}) = \frac{\int_0^\infty \sigma_x(285.5\text{ eV})\rho_{C=C}(z) \exp\left\{-\frac{z}{\lambda\cos\phi}\right\} dz}{\int_0^\infty \sigma_x(320.0\text{ eV})\left\{\sum_i \rho_i(z)\right\} \exp\left\{-\frac{z}{\lambda\cos\phi}\right\} dz} \quad (6)$$

Next, if we assume that the total areal density of C atoms

$$\sum_i \rho_i(z)$$

is independent of z,[57] then we get

$$I_a\lambda\cos\phi = \frac{\sigma_x(285.5\text{ eV})}{\sigma_x(320.0\text{ eV})} \int_0^\infty \frac{\rho_{C=C}(z)}{\sum_i \rho_i} \exp\left\{-\frac{z}{\lambda\cos\phi}\right\} dz$$

$$= \frac{\sigma_x(285.5\text{ eV})}{\sigma_x(320.0\text{ eV})} \int_0^\infty f_{C=C}(z) \exp\left\{-\frac{z}{\lambda\cos\phi}\right\} dz \quad (7)$$

where $f_{C=C}(z)$ is the fraction of C atoms that are in the phenyl

(54) Lin, F.-Y.; Chen, W.-Y.; Hearn, M. T. W. *J. Mol. Recognit.* **2002**, *15*, 55−93.

(55) A continuum state, or vacuum level, is the final state of a C 1s photoionization process resulting in the formation of a free electron and an ion.

(56) At 320 eV, the photon energy is well above any C 1s to π^* or σ^* transition energy. Thus, the X-ray absorption cross section is not expected to be sensitive to the details of the chemical bonding to the C atom and will be the same as the C 1s photoionization cross section.

(57) An assumption that is not strictly valid because of the block architecture and surface segregation of the copolymer, but not completely unrealistic.

rings. From the known normalized PEY of the 1s → $\pi^*_{C=C}$ transition for a pure polystyrene film (with a uniform distribution of phenyl ring C atoms throughout the depth of the film), the ratio of the X-ray absorption coefficients at 320.0 and 285.5 eV can be determined, using eq 7 where $f_{C=C}(z) = 0.75$,[58] to be about 0.14. Thus, knowing the concentration profile, $f_{C=C}(z)$, the NEXAFS escape depth, λ, and the emission angle, ϕ, the normalized PEY can be calculated. Conversely, the concentration profile can be obtained from the inverse Laplace transform of the experimentally determined normalized PEY.

Sampling and Escape Depths in NEXAFS Spectroscopy. Sampling depth is defined as the depth within which a majority of the electrons that are detected (at a given emission angle) originate. For electron emission along the surface normal, most of the electrons that contribute to the electron yield originate from within the electron escape depth—the depth at which the probability of an electron escaping without energy loss drops to $1/e$ (∼37%)—usually approximated by the IMFP, λ. Using the attenuation of the intensity of 1s → σ^*_{C-H} peak by the overlying fluoroalkyl segments of a self-assembled monolayer of $-O_{1.5}Si-(CH_2)_2-(CF_2)_8F$ on silicon, Genzer et al.[46] have determined the value of the escape depth to be 2.43 nm at an EGB of −150 V. This value is significantly higher than the IMFP for Auger electrons with a kinetic energy of 280 eV,[59] which is calculated to be 1.03 nm using eqs 1 and 2. The difference can be reconciled considering the following two facts. First, the channeltron PEY detector detects all Auger electrons that have either lost no energy or have lost energy by inelastic collisions but are still sufficiently energetic to overcome the repulsive force of the negative EGB of the detector. Second, Genzer et al. have used normalized PEY values obtained using an electron emission angle, ϕ, of 85° (cf. Figure 7b). At such high emission angles, the contribution of elastically scattered electrons to the electron yield becomes significant.[60] An electron emitted from a point deeper within the film, which would normally not have reached the detector following a straight-line path, is nevertheless detected because of a shorter route to the detector by elastic scattering events. Because relatively few electrons emerge directly at these large electron emission angles (the depth and thus number of C atoms sampled is small), these elastically scattered electrons become increasingly important and yield incorrect depth profile results if not accounted for. In conclusion, an escape depth of 2.43 nm is most likely an overestimatioin of λ but was nevertheless used to calculate the data points in Figure 9 for want of a more accurate value.

Supporting Information Available: Gel permeation chromatography, IR and NMR spectra of the block copolymer with amphiphilic side chains and its precursors, MALDI-TOF spectrum of the ethoxylated fluoroalkyl surfactant, roughness profile of surfaces used for biofouling assays, images of *Ulva* biofilms on the test surfaces before and after exposure to water shear stress. This material is available free of charge via the Internet at http://pubs.acs.org.

LA052978L

(58) Six of the eight C atoms of styrene are from the phenyl ring. Hence, in a PS film with no concentration variations with depth, the number fraction of phenyl ring C atoms is 0.75. The normalized PEY for the C 1s → $\pi^*_{C=C}$ transition was experimentally found to be about 5.4.

(59) An energy approximately 10 eV below the C 1s ionization energy and corresponding roughly to the energy difference between the HOMO and the C 1s atomic orbital. The actual kinetic energy would be lower than 280 eV by the energy required to remove the Auger electron from the valence band to vacuum.

(60) Cumpson, P. J.; Seah, M. P. *Surf. Interface Anal.* **1997**, *25*, 430−446.

Anti-Biofouling Properties of Comb-Like Block Copolymers with Amphiphilic Side-Chains

Sitaraman Krishnan, Ramakrishnan Ayothi, Alexander Hexemer, John Finlay, Karen E. Sohn, Ruth Perry, Christopher K. Ober, Edward J. Kramer, Maureen E. Callow, James A. Callow, Daniel A. Fischer

Supporting Information

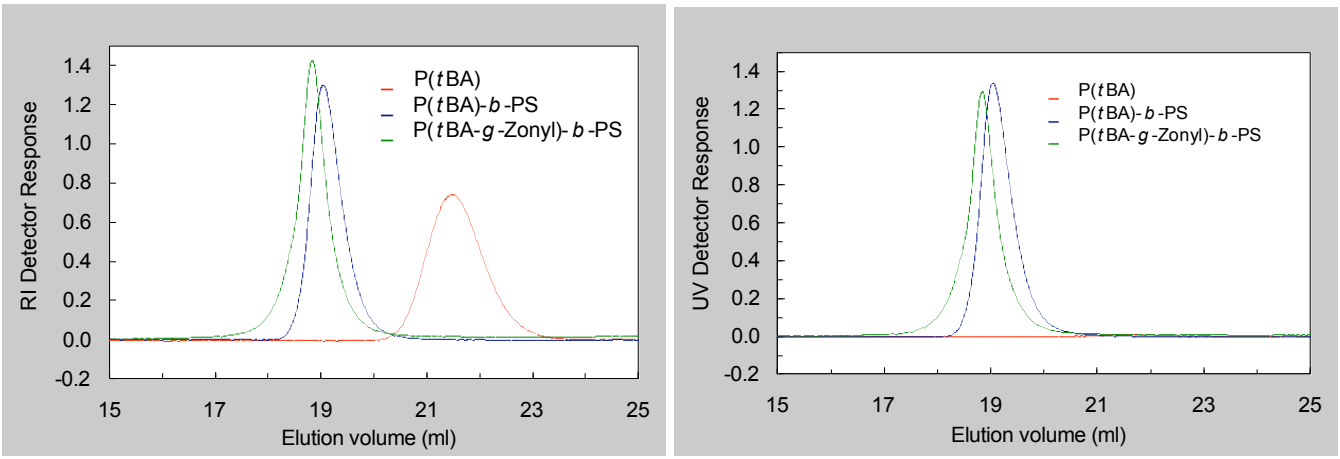

Figure 1. Gel Permeation Chromatography elugrams of poly(*tert*-butyl acrylate) (—), poly(*tert*-butyl acrylate)-*block*-polystyrene (—) and poly(ethoxylated fluoroalkyl acrylate)-*block*-polystyrene (—) in THF at 40 °C. The polydispersity indices of the three polymers were 1.08, 1.16 and 1.31, respectively.

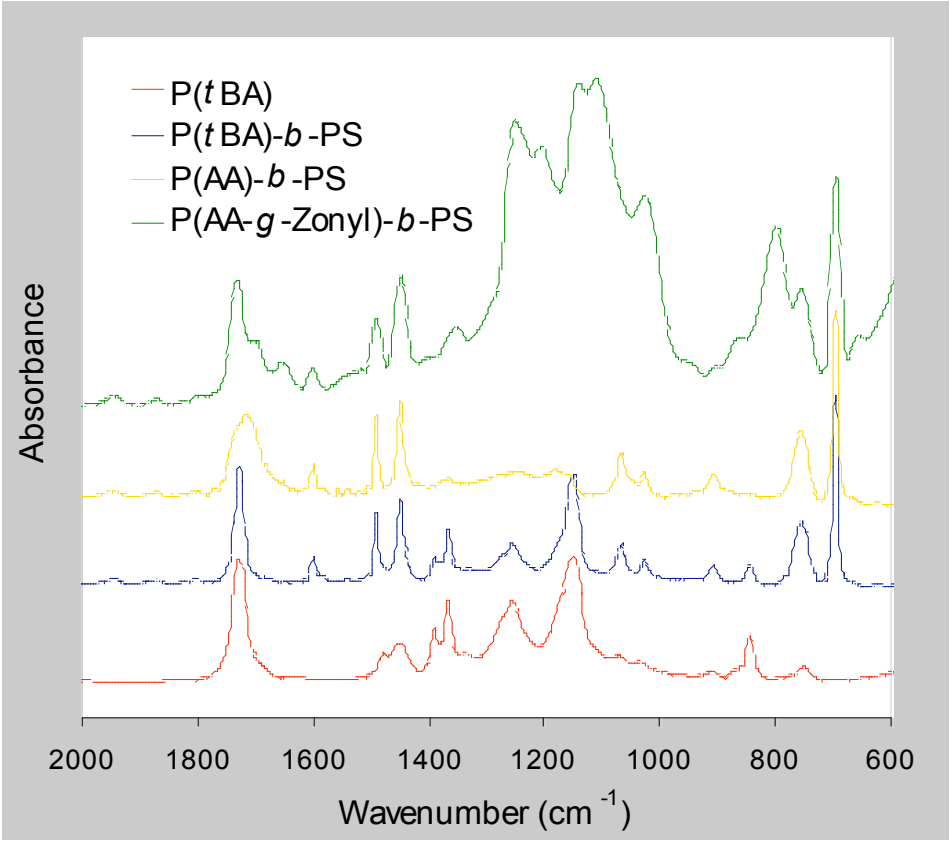

Figure 2. IR spectra of poly(*tert*-butyl acrylate) (—), poly(*tert*-butyl acrylate)-*block*-polystyrene (—),poly(acrylic acid)-*block*-polystyrene (—) and poly(ethoxylated fluoroalkyl acrylate)-*block*-polystyrene (—).

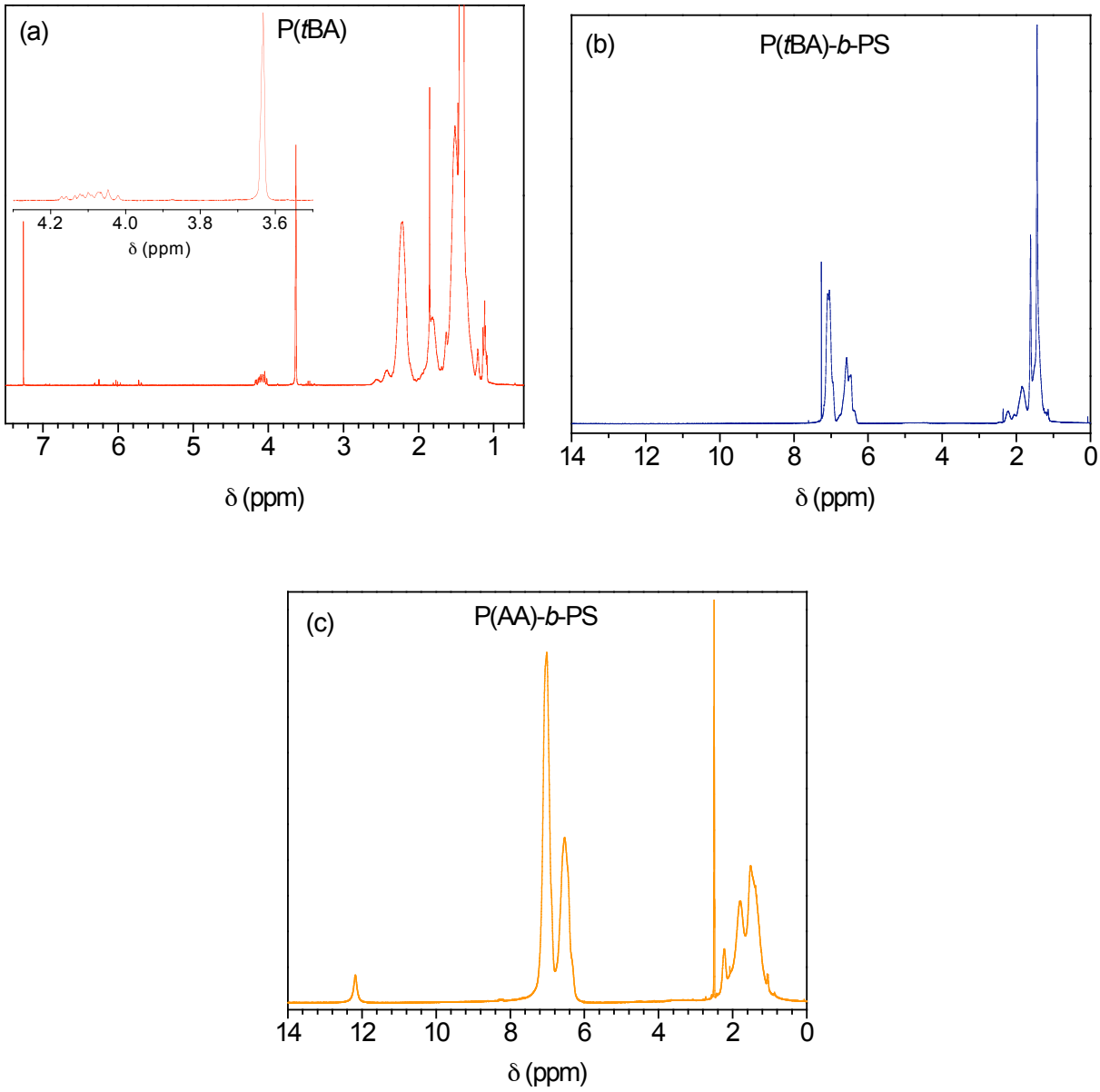

Figure 3. ^{1}H NMR spectra (300 MHz) of (a) poly(*tert*-butyl acrylate) in $CDCl_3$, (b) poly(*tert*-butyl acrylate)-*block*-polystyrene in $CDCl_3$, (c) poly(acrylic acid)-*block*-polystyrene in DMSO-d_6.

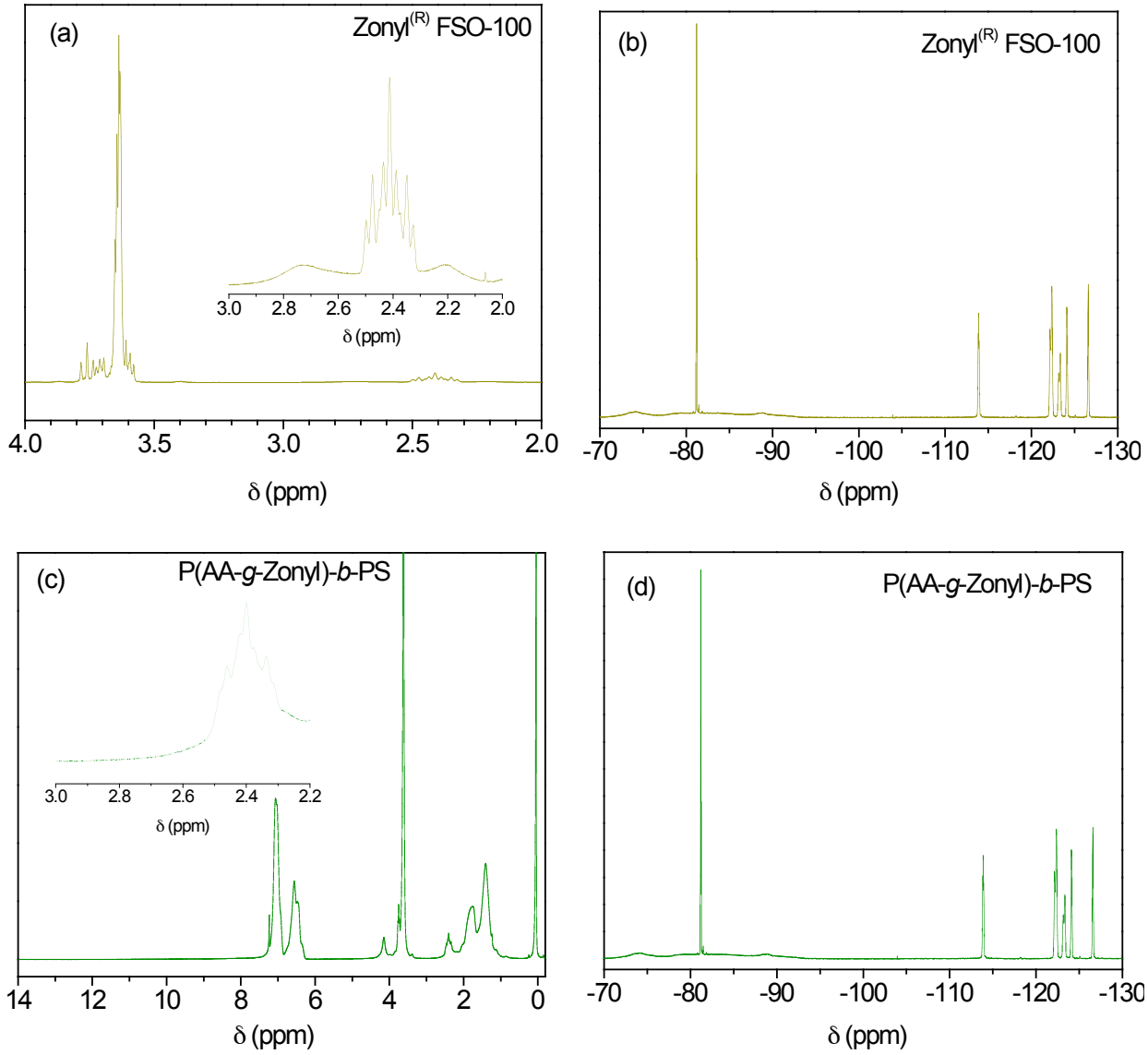

Figure 4. (a) ^{1}H NMR (300 MHz) of Zonyl® FSO-100 in $CDCl_3$, (b) ^{19}F NMR (282.24 MHz) of Zonyl® FSO-100 in $CDCl_3$, (c) ^{1}H NMR (300 MHz) of poly(ethoxylated fluoroalkyl acrylate)-*block*-polystyrene in $CDCl_3$, and (d) ^{19}F NMR (282.24 MHz) of poly(ethoxylated fluoroalkyl acrylate)-*block*-polystyrene in $CDCl_3$.

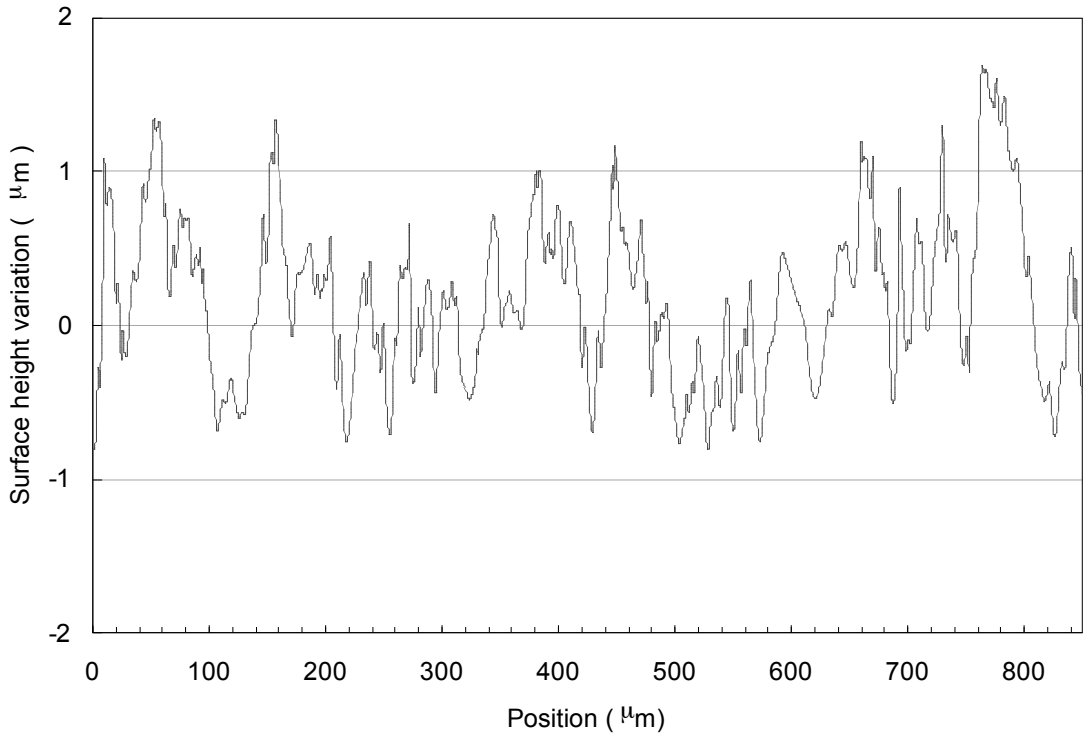

Figure 5. Height profile of a spray-coated surface of the amphiphilic block copolymer; bilayer coating on a glass microscope slide annealed at 60 °C.

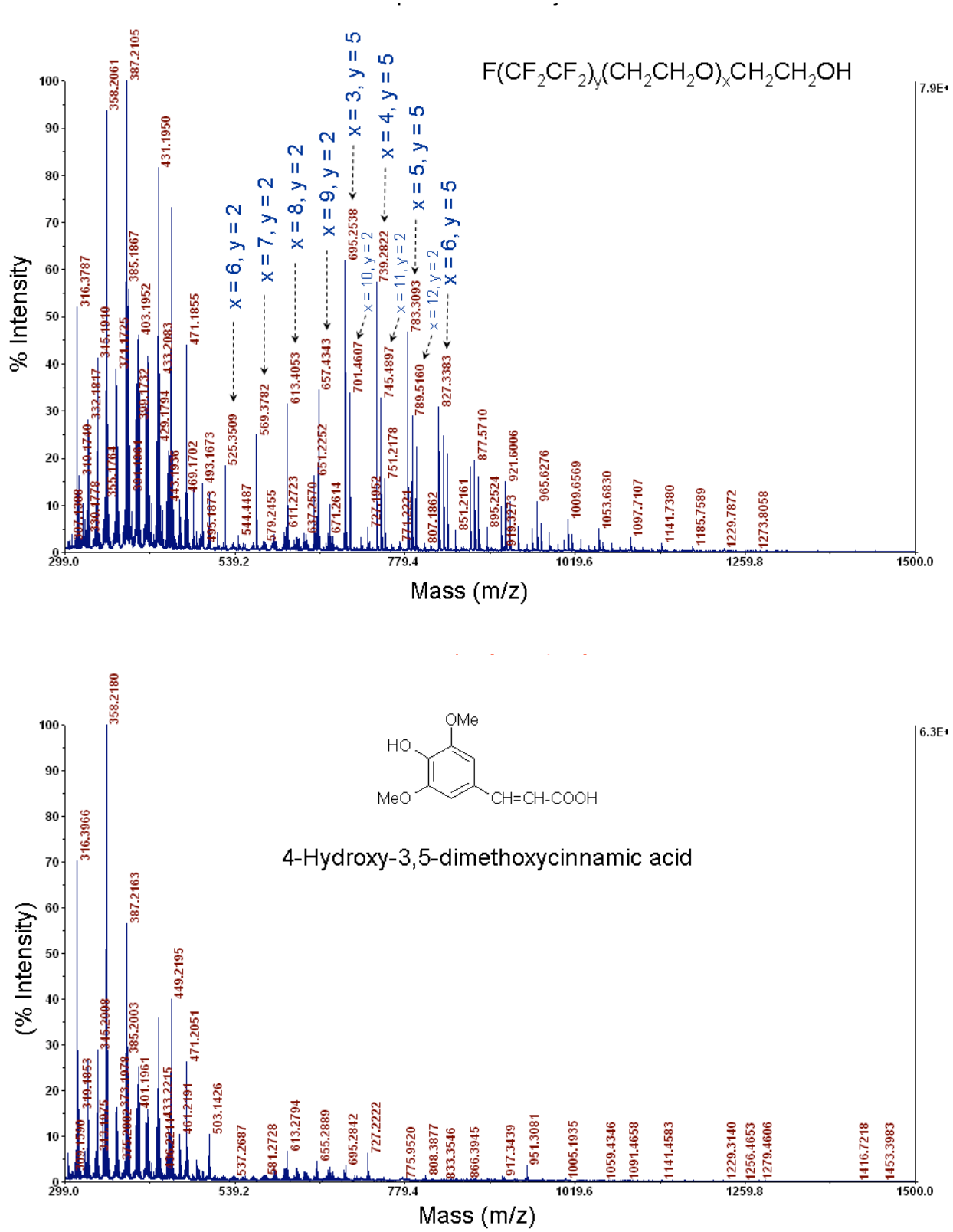

Figure 6. MALDI-TOP spectrum of Zonyl® FSO-100 (top) and the blank matrix (bottom).

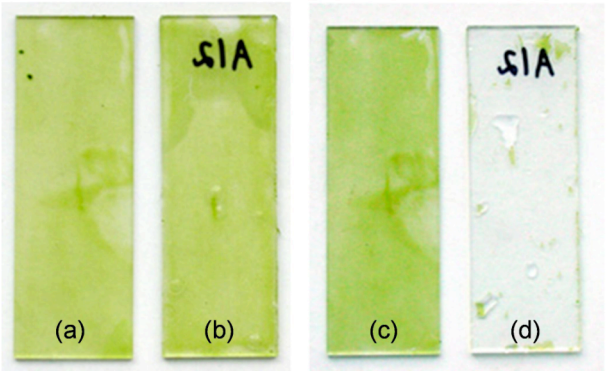

Figure 7. Images of 8 day *Ulva* biofilms; (a) glass and (b) A60 surfaces before water flow; (c) glass and (d) A60 after exposure to shear stress of 53 Pa in water channel. Spore settlement density = 0.1 (OD 660 nm).

Determination of x and y values for $F(CF_2CF_2)_y(CH_2CH_2O)_xCH_2CH_2OH$ and poly(ethoxylated fluoroalkyl acrylate)-*block*-polystyrene using NMR.

Let $A_{F,tot}$ denote the sum of areas under all the peaks in the ^{19}F NMR spectrum, and A_{CF_3}, the area under the peak corresponding to $-CF_3$ fluorine atoms. Then,

$$y = \frac{1}{4}\left(\frac{3A_{F,tot}}{A_{CF_3}} - 1\right)$$

Let $A_{H,tot}$ denote the sum of the areas under all the peaks corresponding to the ethoxylated fluoroalkyl side-chains in the ^1H NMR spectrum, and $A_{CH_2CF_2}$, the area under the peak corresponding to $-CH_2CF_2-$ protons. Then,

$$x = \frac{1}{4}\left(\frac{2A_{H,tot}}{A_{CH_2CF_2}} - 5\right)$$